

Pseudogaps in the t - J model: An extended dynamical mean-field theory studyK. Haule,^{1,4} A. Rosch,² J. Kroha,³ and P. Wölfle²¹*Department of Physics and Astronomy, Rutgers University, 136 Frelinghuysen Road, Piscataway, New Jersey 08854-8019, USA*²*Institut für Theorie der Kondensierten Materie, Universität Karlsruhe, D-76128 Karlsruhe, Germany*³*Physikalisches Institut, Universität Bonn, Nussallee 12, 53115 Bonn, Germany*⁴*J. Stefan Institute, 1000 Ljubljana, Slovenia*

(Received 4 April 2003; revised manuscript received 10 June 2003; published 28 October 2003)

We investigate the highly incoherent regime of hole-doped two-dimensional Mott-Hubbard insulators at moderately small doping δ and temperatures $\geq 0.1J$, where J is the exchange coupling. Within an extended dynamical mean-field theory of the t - J model and a generalized noncrossing approximation we calculate the single-particle spectral function, the dynamical susceptibility, and thermodynamic and transport quantities. Short-ranged antiferromagnetic fluctuations lead to strongly incoherent single-particle dynamics, large entropy, and large electrical resistivity. At low doping a pseudogap is found to open up in both the single-particle and spin excitation spectra, leading to a decrease in entropy and resistivity. The Hall coefficient changes sign to positive values upon lowering the doping level and increases inversely proportional to δ .

DOI: 10.1103/PhysRevB.68.155119

PACS number(s): 71.30.+h, 74.72.-h, 71.10.Hf

I. INTRODUCTION

Strongly interacting Fermi systems on a two-dimensional (2D) lattice have been a focus of interest ever since high-temperature superconductor materials were discovered in 1986. The unusual properties of these materials, in particular in the normal conducting phase, have led to the hypothesis that the usual Landau Fermi liquid theory may not be applicable in this case.¹ A widely accepted view holds that these systems may be considered as hole-doped Mott-Hubbard insulators. The correlations present in a Mott-Hubbard insulator are characterized by strongly suppressed charge fluctuations (due to the constrained hopping of the holes resulting from the strong on-site Coulomb repulsion U) and enhanced quantum spin fluctuations governed by the antiferromagnetic nearest-neighbor spin exchange interaction. The interplay of the motion of holes with the antiferromagnetically correlated spin background is the central problem of hole-doped Mott-Hubbard insulators. Despite an extraordinary effort by many theorists and a correspondingly large number of papers we believe it to be fair to say that a thorough understanding of this problem is still lacking.

The ground state of the Mott insulating state of electrons on a square lattice at half-filling is expected to be antiferromagnetically ordered.^{2,3} Doping with holes leads to a rapid destruction of long-range order, at a critical concentration δ_c of a few percent doping. For larger dopings there is evidence for strong antiferromagnetic spin fluctuations of relatively short range.

In this paper we undertake to explore the consequences of strong incoherent and local (i.e., nearest-neighbor) spin fluctuations on the dynamics of charge carriers and on the thermodynamics of the systems. We also investigate how the single-particle properties feed back into the spin dynamics. Our approach is focused on the temperature regime of $0.1J \leq T \leq t$ ($J=0.3t$ in the cuprates) where J is the exchange constant and t is the nearest-neighbor hopping amplitude. In this regime we expect strong quantum and thermal fluctuations driven by competing interactions to decohere the fer-

mionic excitations. This temperature regime is bounded from below by possible antiferromagnetic, superconducting, or other ordered states. The incoherent regime characterized by a large single-particle decay rate $\text{Im} \Sigma \sim t$ is confined to small doping levels $\delta_c \lesssim \delta \lesssim 0.3$ and crosses over into a Fermi liquid state at $\delta \geq 0.3$.

A minimal model encompassing the physics described above is the t - J model. It is well known that the interplay of hopping and local correlations induced by the on-site Coulomb interaction may be captured in dynamical mean-field theory, in which the lattice model is mapped onto a quantum impurity coupled to a fermionic bath in a self-consistent fashion.^{4,5} In the same spirit the nearest-neighbor exchange interaction of a given spin to its neighboring spins may be approximated by a dynamically fluctuating bosonic field, to be determined self-consistently.^{6,7} In this way the two principal processes—constrained hopping and spin exchange interaction—may be fully incorporated on the same footing, on the level of short-range correlations.

As reviewed in Sec. II, the extended dynamical mean-field theory (EDMFT) for the two-dimensional t - J model is obtained by approximating the single-particle self-energy $\Sigma_{\mathbf{k}}(\omega)$ and the two-particle self-energy $M_{\mathbf{q}}(\omega)$ by momentum-independent functions. $\Sigma(\omega)$ and $M(\omega)$ are obtained by equating the local (i.e., the momentum-integrated) single-particle Green's function and spin susceptibility, respectively, with the corresponding quantities of an extended Anderson impurity model, featuring a fermionic and a bosonic bath to be determined self-consistently. For the bare hopping integrals and exchange couplings we use a nearest-neighbor tight-binding model on the square lattice. The local approximation is better the higher the spatial dimension d and becomes exact for $d \rightarrow \infty$, provided the hopping amplitude t and the exchange coupling J are scaled as t/\sqrt{d} and J/\sqrt{d} . This scaling is possible in the paramagnetic regime. Most of the methods employed for the solution of the Anderson impurity or Kondo problem do not work here. We use self-consistent perturbation theory in the form of conserving

approximations^{8,9} and the exact projection onto the Hilbert space without double occupancy (limit $U \rightarrow \infty$). We are interested in describing the highly incoherent regime at small doping levels and not too low temperatures, where the spectral functions are broad and relatively featureless. In this regime we expect vertex corrections and higher-order processes, in general, to change the characteristic parameters like maximum values, peak widths, and gap widths of the dynamic quantities by correction terms of order unity, but we do not expect that these contributions lead to more coherence or new collective behavior. In this spirit we approximate all self-energies by their lowest order self-consistent perturbation theory expressions (in the hopping parameter and exchange coupling). The resulting theory, presented in Sec. III, is an extension of the non-crossing approximation¹⁰ (NCA) including the bosonic bath.

The results of this approximation scheme for the t - J model are presented in Sec. IV. It turns out that nearest-neighbor spin fluctuations are sufficient to create a pseudogap in the single-particle spectrum and in the spin excitation spectrum at q vectors away from (π, π) , for small dopings $\delta \leq 0.1$, similar to what is seen in angle-resolved photoemission spectroscopy (ARPES) experiments¹¹ and in the magnetic properties.^{12,13} The pseudogap scales with J . There are several indications that Fermi liquid behavior is violated for $\delta \leq 0.2$. Most noteworthy, the effective chemical potential is found to move from the center of the band up to the band edge, as the doping is decreased to small values. As δ grows beyond 0.25, however, Fermi liquid behavior appears to be restored. The entropy turns out to be large in the range $0.1 \leq \delta \leq 0.2$ and is reduced on both sides of this interval by the pseudogap and incipient Fermi liquid behavior, respectively. The resistivity is dominated by strong incoherent scattering, and the Hall coefficient is found to be hole like, $\propto 1/\delta$, for small δ , again resembling the observed behavior.¹⁴ Finally we note that in dimensions less or equal to 2, EDMFT does not allow for a continuous phase transition to an antiferromagnetically ordered state at any finite temperature, in accordance with the Mermin-Wagner theorem, as this would require the static local spin susceptibility to diverge and this is forbidden by its self-consistent coupling within EDMFT (see discussion in Sec. V). Some of the results have been reported in Ref. 15.

Results similar to ours have been found in two recent works using DMFT for a cluster of sites within the Hubbard model. Maier *et al.*¹⁶ applied the dynamical cluster approximation (DCA) for various cluster sizes up to 64 sites to the Hubbard model in the intermediate-coupling regime ($U \sim$ bandwidth). The DCA equations were solved with quantum Monte Carlo (QMC) techniques down to room temperature. The authors of Ref. 16 identified signals for non-Fermi-liquid behavior at low doping $\delta \leq 0.1$ and found a large residual scattering rate and a pronounced pseudogap at low doping. In Ref. 17, Stanescu and Phillips studied the Hubbard model at intermediate coupling within a two-site cluster approach using the noncrossing approximation as a quantum impurity solver at not too low temperatures. It is again found that Luttinger's theorem appears to be violated for low doping in a regime where a pseudogap opens.

Despite the similarity of the numerical results, quite different explanations for the observed pseudogap physics have been suggested, ranging from short-range spin correlations, spin-charge separation, and resonant valence bond (RVB) physics¹⁶ to effects of the upper Hubbard band and current correlations involving three neighboring sites.¹⁷ By construction our approximation scheme is not able to describe such intersite correlations or RVB singlets and does not include the upper Hubbard band: nevertheless, the overall results are qualitatively very similar. We take this as a strong indication that neither short-range magnetic or current correlations nor RVB physics is the underlying reason but argue that there is another generic mechanism for pseudogap formation: The strongly incoherent dynamics captured in our scheme as well as those of Refs. 16 and 17 appears to be the dominant feature of the Hubbard model as well as the t - J model in the low-energy sector ($0.1J \leq \omega \leq t$) for small doping. Therefore pseudogap formation seems to be a generic property of any strongly incoherent Fermi system close to a Mott insulator. In other words, the existence of a pseudogap neither requires slowly fluctuating, finite-range-ordered domains (antiferromagnetic, superconducting),¹⁸ nor a local resonance state.

II. EXTENDED DYNAMICAL MEAN-FIELD THEORY OF THE T - J MODEL

The standard model embodying the physics of the hole-doped Mott-Hubbard insulator is the t - J model, defined by the Hamiltonian

$$H = \sum_{i,j} t_{ij} \tilde{c}_{i\sigma}^\dagger \tilde{c}_{j\sigma} + \frac{1}{2} \sum_{i,j} J_{ij} \mathbf{S}_i \cdot \mathbf{S}_j, \quad (1)$$

where $\mathbf{S}_i = \frac{1}{2} \sum_{\sigma,\sigma'} \tilde{c}_{i\sigma}^\dagger \boldsymbol{\tau}_{\sigma\sigma'} \tilde{c}_{i\sigma'}$ is the spin operator at lattice site i , $\boldsymbol{\tau}$ denotes the vector of Pauli matrices, and t_{ij} (J_{ij}) are the hopping amplitudes (exchange interaction) connecting sites i and j . For the numerical evaluation to be discussed later we will use a tight-binding model on a two-dimensional square lattice, $t_{ij} = -t \delta_{i,i+\tau}$, $J_{ij} = J \delta_{i,i+\tau}$, where τ labels nearest-neighbor sites. The operator $\tilde{c}_{i\sigma}^\dagger$ ($\tilde{c}_{i\sigma}$) creates (annihilates) an electron at site i with spin projection σ at a singly occupied lattice site. In terms of usual electron operators $c_{i\sigma}^\dagger$ ($c_{i\sigma}$) one has $\tilde{c}_{i\sigma}^\dagger = c_{i\sigma}^\dagger (1 - n_{i,-\sigma})$, where $n_{i\sigma} = c_{i\sigma}^\dagger c_{i\sigma}$ is the occupation number operator. In this way occupation of lattice sites by two electrons with spins \uparrow and \downarrow is avoided, which would cost the large Hubbard energy U . We will be interested in electron densities close to half-filling of the band, such that $\langle \sum_{\sigma} n_{i\sigma} \rangle = n = 1 - \delta$, where $\delta \ll 1$ is the doping concentration of holes.

Whereas at exactly half-filling, when H reduces to the Heisenberg model, the ground state has antiferromagnetic long-range order, we anticipate that this will not be the case for sufficiently large doping $\delta > \delta_c$ (in experiment $\delta_c \approx 0.03$ for low T) or large T . In this regime it is reasonable to assume the antiferromagnetic correlations in the system to be short ranged. We assume furthermore that additional forms of long-range order (such as superconductivity) that may be possible ground states of the t - J model are confined to a lower-temperature regime, such that the corresponding fluc-

tuations are subdominant at elevated temperatures. Consequently, one expects an extended high-temperature regime where short-ranged spin fluctuations lead to a highly incoherent metallic state, as observed in high-temperature superconductors, with anomalous transport properties (large, non-Fermi-liquid-type electrical resistivity, holelike Hall constant), large entropy, broad “quasiparticle” peaks in photoemission, etc. It is our aim to investigate this regime within an approximation scheme which neglects most of the longer-range spatial correlations, but keeps the dominant short-range spin correlations.

The single-particle dynamics and two-particle dynamics of the model are described by the Green’s function

$$G_{\mathbf{k},\sigma}(i\omega) = - \int_0^\beta d\tau e^{i\omega\tau} \langle T_\tau \tilde{c}_{\mathbf{k}\sigma}(\tau) \tilde{c}_{\mathbf{k}\sigma}(0) \rangle$$

$$= \frac{1}{i\omega + \mu - \epsilon_{\mathbf{k}} - \Sigma_{\mathbf{k},\sigma}(i\omega)} \quad (2)$$

and by the spin susceptibility

$$\chi_{\mathbf{q},\alpha}(i\Omega) = \int_0^\beta d\tau e^{i\Omega\tau} \langle T_\tau S_{-\mathbf{q},\alpha}(\tau) S_{\mathbf{q},\alpha}(0) \rangle$$

$$= \frac{1}{J_{\mathbf{q}} + M_{\mathbf{q},\alpha}(i\Omega)}. \quad (3)$$

Here β is the inverse temperature T (we employ units with $k_B = \hbar = 1$), ω and Ω are fermionic and bosonic Matsubara frequencies, and $\epsilon_{\mathbf{k}}$ and $J_{\mathbf{q}}$ are the lattice Fourier transforms of the hopping amplitudes t_{ij} and the exchange couplings J_{ij} , respectively. While the self-energies $\Sigma_{\mathbf{k}}(i\omega)$ and $M_{\mathbf{q}}(i\omega)$ are momentum dependent in general, the observation that the fluctuations in the system are short ranged in the regime we are interested in suggests that a “local” approximation, neglecting the momentum dependence of Σ and M altogether, may be a good starting point. We therefore employ in this paper the main approximation

$$\Sigma_{\mathbf{k}}(\omega) \simeq \Sigma(\omega) \quad (4)$$

and

$$M_{\mathbf{q}}(\omega) \simeq M(\omega), \quad (5)$$

thus capturing the effect of local fluctuations in time, which we expect to be important in the presence of strong inelastic scattering.

The momentum independence of Σ and M allows us to map the lattice problem onto an Anderson impurity problem where the host medium has to be determined self-consistently. Considering first the single-particle properties—i.e., $\Sigma(\omega)$ —the corresponding DMFT has been widely used to calculate properties of the Hubbard model and periodic Anderson model.^{4,5} One maps the problem onto an Anderson impurity embedded in a fermionic bath. Applied to the t - J model it amounts to treating the exchange interaction in mean-field theory. This is not sufficient to allow us to maintain the balance between dynamical hopping processes and spin fluctuations, which is at the heart of the t - J model. We

therefore follow Refs. 6 and 7 and extend the dynamical mean-field idea for the paramagnetic phase by introducing a fluctuating magnetic field coupling to the local spin as representing an additional class of degrees of freedom of the medium. This type of approximation, termed “extended DMFT,” has been applied to the Kondo lattice model⁶ and the extended Hubbard model.⁷ It is important to note that EDMFT (i.e., the neglecting of the momentum dependences of Σ and M) becomes exact in the limit of infinite dimensions $d \rightarrow \infty$, provided t and J are scaled as t/\sqrt{d} and J/\sqrt{d} , respectively. We shall use this property in deriving the EDMFT equations (see Appendix A). We will, however, regard EDMFT as an approximation applied in finite dimensions and, as such, will use the tight-binding expressions for $\epsilon_{\mathbf{k}}$ and $J_{\mathbf{q}}$ valid in $d=2$.

To summarize, the EDMFT is probably best visualized by considering a single-site, the “impurity,” and its coupling to the surrounding “medium.” There are two types of coupling processes, as is evident from the Hamiltonian

(i) Hopping to and from the “impurity” into the medium, as in the Anderson impurity model (in the limit of infinite U , as a consequence of the no double occupancy constraint). The medium is modeled by a noninteracting fermion system (the “conduction electrons”), whose local density of states has to be determined self-consistently.

(ii) Exchange coupling of the local spin at the “impurity” site to the spins of the medium. In the limit $d \rightarrow \infty$ the two components of the medium—fermions (see above) and spin fluctuations—are completely decoupled. We do not expect that this approximation holds in 2D for low temperatures. But in the regime considered in this paper, where electrons are highly incoherent, we believe that such a modeling is appropriate. The spin fluctuations of the medium are described by a (vector) bosonic bath, whose spectrum again has to be determined self-consistently.

In this way one is led to a generalized quantum impurity model with Hamiltonian

$$H_{\text{EDMFT}} = \sum_{k\sigma} E_k c_{k\sigma}^\dagger c_{k\sigma} + V \sum_{k\sigma} (c_{k\sigma}^\dagger \tilde{d}_\sigma + \text{H.c.}) - \mu n_d$$

$$+ \sum_{\mathbf{q}} \omega_{\mathbf{q}} \mathbf{h}_{\mathbf{q}} \cdot \mathbf{h}_{\mathbf{q}} + I \sum_{\mathbf{q}} \mathbf{S}_d \cdot (\mathbf{h}_{\mathbf{q}} + \mathbf{h}_{-\mathbf{q}}). \quad (6)$$

A formal derivation of H_{EDMFT} in the limit $d \rightarrow \infty$ is given in Appendix A. Here \tilde{d}_σ^\dagger is a projected fermion creation operator for the impurity orbital (the original operator $\tilde{c}_{0\sigma}^\dagger$ at the chosen “impurity” site 0), $n_d = \sum_\sigma \tilde{d}_\sigma^\dagger \tilde{d}_\sigma$, and $\mathbf{S}_d = \frac{1}{2} \sum_{\sigma,\sigma'} \tilde{d}_\sigma^\dagger \boldsymbol{\tau}_{\sigma\sigma'} \tilde{d}_{\sigma'}$. The fermionic bath is represented by free fermion operators $c_{k\sigma}^\dagger$, the bosonic bath by free boson operators $h_{q\alpha}^\dagger$, $\alpha=1,2,3$ with $\mathbf{h}_{\mathbf{q}} = (h_{q1}, h_{q2}, h_{q3})$, and $\Sigma_{\mathbf{q}}(\mathbf{h}_{\mathbf{q}} + \mathbf{h}_{-\mathbf{q}})$ plays the role of a fluctuating local magnetic field. The excitation spectrum of the bath degrees of freedom, E_k and $\omega_{\mathbf{q}}$, as well as the coupling constants V and I have to be determined self-consistently by equating both the single-particle Green’s function and the spin susceptibility of

the impurity model G_{imp}, χ_{imp} with the local Green's function G_{loc} and the local susceptibility χ_{loc} of the lattice model,

$$G_{imp,\sigma}(i\omega) = - \int_0^\beta d\tau e^{i\omega\tau} \langle T_\tau \tilde{d}_\sigma(\tau) \tilde{d}_\sigma^\dagger(0) \rangle = G_{loc}(i\omega),$$

$$\chi_{imp,\alpha}(i\omega) = \int_0^\beta d\tau e^{i\omega\tau} \langle T_\tau S_\alpha(\tau) S_\alpha(0) \rangle = \chi_{loc}(i\omega). \quad (7)$$

The local G and χ are obtained from their lattice counterparts (2) and (3), taking into account Eqs. (4) and (5), and by summation over all momenta:

$$G_{loc}(\omega) = \sum_{\mathbf{k}} G_{\mathbf{k}}(i\omega), \quad (8)$$

$$\chi_{loc}(\omega) = \sum_{\mathbf{q}} \chi_{\mathbf{q}}(i\omega). \quad (9)$$

As shown in Appendix A, the self-energies Σ and M also characterize the impurity Green's functions

$$G_{imp}(i\omega) = [i\omega + \mu - V^2 G_c(i\omega) - \Sigma(i\omega)]^{-1}, \quad (10)$$

$$\chi_{imp}(i\omega) = [M - I^2 G_h]^{-1}, \quad (11)$$

where

$$G_c(i\omega) = \sum_{\mathbf{k}} \frac{1}{i\omega - E_{\mathbf{k}}}, \quad (12)$$

$$G_h(i\omega) = \sum_{\mathbf{q}} \frac{2\omega_{\mathbf{q}}}{(i\omega)^2 - (\omega_{\mathbf{q}})^2}, \quad (13)$$

so that the system of equations (2)–(11) is closed. It follows from Eqs. (10) and (11) that only the densities of states of the baths,

$$A_c(\omega) = \frac{V^2}{\pi} \text{Im} G_c(\omega - i0) = V^2 \sum_{\mathbf{k}} \delta(\omega - E_{\mathbf{k}}) \quad (14)$$

and

$$D_h(\omega) = \frac{I^2}{\pi} \text{Im} G_h(\omega - i0)$$

$$= I^2 \sum_{\mathbf{q}} [\delta(\omega - \omega_{\mathbf{q}}) - \delta(\omega + \omega_{\mathbf{q}})], \quad (15)$$

are needed. For practical purposes we have included the coupling constants V and I , respectively, in the definitions of the density of states.

III. GENERALIZED NONCROSSING APPROXIMATION

The solution of the quantum impurity model (6) for given $A_c(\omega)$ and $D_h(\omega)$ is difficult. Many of the methods developed in the past for solving Anderson impurity models in the context of DMFT such as iterated perturbation theory⁵ and

the numerical renormalization group method¹⁹ are not applicable in the case of a bosonic bath. The quantum Monte Carlo method has been successfully applied to solve the EDMFT problem for an anisotropic Kondo lattice model with Ising-type spin coupling,^{20,21} but it is extremely difficult to treat Heisenberg couplings with manageable effort. The only method left to us is self-consistent perturbation theory like the NCA or the conserving T -matrix approximation (CTMA).^{9,10}

We will therefore employ a conserving diagrammatic approximation in which infinite classes of perturbation theory in V and I are resummed. We are aiming at a level of approximation corresponding to the NCA for the usual Anderson model. A convenient way to phrase the perturbation theory in the hopping V and the exchange coupling I , in the presence of an infinitely strong Coulomb repulsion U , is in terms of a pseudoparticle representation. We define pseudofermion operators $f_\sigma^\dagger, \sigma = \uparrow, \downarrow$, creating the singly occupied impurity state and the slave boson operator b^\dagger creating the empty impurity level, when acting on a corresponding vacuum state.²² Since the local level is either empty or singly occupied, the operator constraint $Q = b^\dagger b + \sum_{\sigma} f_\sigma^\dagger f_\sigma = 1$ has to be satisfied at all times. The constraint is enforced exactly by adding a term λQ to the Hamiltonian and taking the limit $\lambda \rightarrow \infty$ [see Eq. (23) below]. The projected local electron operators \tilde{d}_σ may then be replaced by $b^\dagger f_\sigma$, turning the problem into a many-body system of pseudofermions f_σ and slave bosons b , interacting with the fermions $c_{k\sigma}$ and bosons $\mathbf{h}_{\mathbf{q}}$ of the bath.

It is essential for any approximation scheme to respect the projection and not to allow transitions between different sectors of Hilbert space labeled by Q . To this end we employ a conserving approximation specified by a generating Luttinger-Ward-type functional Φ from which all self-energies are obtained as functional derivatives, $\Sigma_a = \delta\Phi/\delta G_a$. The building blocks of Φ are the dressed Green's functions of pseudofermions G_f (depicted as a dashed line), slave bosons G_b (wiggly line), bath fermions G_c (solid line), and bath bosons G_h (curly line) and the vertices corresponding to hopping V and exchange interaction I .

In the strongly incoherent regime we are interested in, vertex corrections are not expected to change the behavior in a qualitative way. They may, however, lead to quantitative changes. In this paper we would like to explore the leading behavior first, so that we may neglect vertex corrections for the moment. The lowest-order terms of Φ in self-consistent perturbation theory in the bare coupling constants V and I are shown in Fig. 1(a). The first one is the known generating functional of the NCA, whereas the second one is new and involves the bath bosons. The corresponding self-energies are shown in Fig. 1(b), for the pseudofermions (Σ_f) and slave bosons (Σ_b), as well as the bath fermions (Σ_c) and the bath bosons (Σ_h). We note that the impurity single-particle Green's function after projection ($\lambda \rightarrow \infty$) is related to Σ_c by⁸

$$G_{imp}(i\omega) = \frac{1}{V^2} \Sigma_c(i\omega) \quad (16)$$

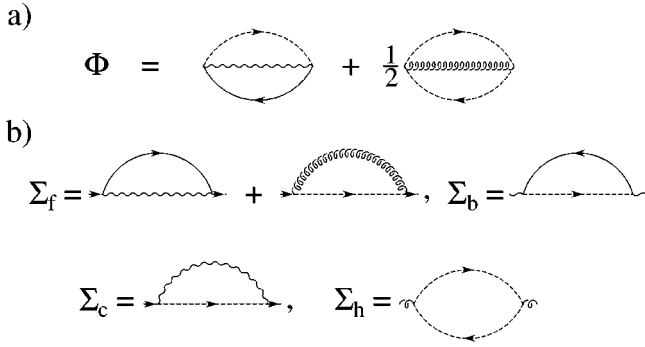


FIG. 1. The two lowest-order contributions to the Luttinger-Ward functional Φ and corresponding self-energies. Only diagrams with no line crossings are taken into account (a generalization of the NCA). The dashed (wavy) line denotes the pseudofermion (pseudoboson) Green's function G_f (G_b), and the solid lines represent the conduction electron Green's functions G_c , the curly line the correlator G_h of the bosonic bath. Also shown are the pseudo-self-energies as well as self-energies of the baths.

and likewise the impurity spin susceptibility is proportional to the bath boson self-energy

$$\chi_{imp}(i\omega) = -\frac{1}{I^2} \Sigma_h(i\omega). \quad (17)$$

Cutting a pseudofermion line in each of the two diagrams of the generating functional, Fig. 1(a), one finds two diagrams for the pseudofermion self-energy

$$\Sigma_f(i\omega) = \Sigma_f^{(2a)}(i\omega) + \Sigma_f^{(2b)}(i\omega) \quad (18)$$

as depicted in Fig. 1(b). Likewise, the slave boson self-energy Σ_b , the fermion bath self-energy Σ_c , and the boson bath self-energy Σ_h are obtained by cutting the respective Green's function lines in the two diagrams of Φ . The corresponding analytical expressions are given by

$$\Sigma_{f\sigma}^{(2a)}(i\omega) = -V^2 T \sum_{\omega'} G_{c\sigma}(i\omega') G_b(i\omega - i\omega'), \quad (19a)$$

$$\begin{aligned} \Sigma_{f\sigma}^{(2b)}(i\omega) &= -\frac{1}{4} I^2 \sum_{\sigma', \alpha} \tau_{\sigma\sigma'}^\alpha \tau_{\sigma'\sigma}^\alpha T \\ &\times \sum_{\Omega} G_{h\alpha}(i\Omega) G_{f\sigma'}(i\omega + i\Omega), \end{aligned} \quad (19b)$$

$$\Sigma_b(i\Omega) = V^2 T \sum_{\sigma, \omega'} G_{c\sigma}(i\omega') G_{f\sigma}(i\Omega + i\omega'), \quad (19c)$$

$$\Sigma_{c\sigma}(i\omega) = -V^2 T \sum_{\Omega} G_{f\sigma}(i\omega + i\Omega) G_b(i\Omega), \quad (19d)$$

$$\begin{aligned} \Sigma_{h\alpha}(i\Omega) &= \frac{1}{4} I^2 \sum_{\sigma, \sigma'} \tau_{\sigma\sigma'}^\alpha \tau_{\sigma'\sigma}^\alpha T \\ &\times \sum_{\omega'} G_{f\sigma}(i\omega') G_{f\sigma'}(i\omega' + i\Omega), \end{aligned} \quad (19e)$$

where $i\omega$, $i\omega'$, and $i\Omega$ are fermionic and bosonic Matsubara frequencies, respectively; $\sigma, \sigma' = \uparrow, \downarrow$; and $\alpha = 1, 2, 3$.

Next one may transform the Matsubara frequency sums into frequency integrals along the branch cuts of the Green's functions and perform the analytical continuation to the real frequency axis. The projection to the singly occupied sector of Hilbert space may now be carried out. To this end the frequency arguments of the pseudoparticle Green's functions are shifted by the chemical potential λ and the limit $\lambda \rightarrow \infty$ is taken. This yields

$$\Sigma_{f\sigma}^{(2a)}(\omega + i0) = \int d\xi f(-\xi) A_{c\sigma}(\xi) G_b(\omega - \xi + i0), \quad (20a)$$

$$\begin{aligned} \Sigma_{f\sigma}^{(2b)}(\omega + i0) &= \frac{1}{4} \sum_{\sigma', \alpha} \tau_{\sigma\sigma'}^\alpha \tau_{\sigma'\sigma}^\alpha \int d\xi n(\xi) \\ &\times D_{h\alpha}(\xi) G_{f\sigma'}(\omega + \xi + i0), \end{aligned} \quad (20b)$$

$$\Sigma_b(\omega + i0) = \sum_{\sigma} \int d\xi f(\xi) A_{c\sigma}(\xi) G_{f\sigma}(\omega + \xi + i0), \quad (20c)$$

where $f(\xi)$ and $n(\xi)$ are the Fermi and Bose functions, respectively, and $A_c(\xi)$ and $D_h(\xi)$ are spectral functions of the fermionic and bosonic baths as defined in Eqs. (14) and (15).

Since we incorporated the factors of V^2 and I^2 into the definition, A_c and D_h are not normalized anymore, their total weight being given by V^2 and I^2 , respectively.

The projected pseudoparticle Green's functions are expressed in terms of their self-energies as

$$G_f(\omega + i0) = \frac{1}{\omega + \mu - \lambda_0 - \Sigma_f(\omega + i0)}, \quad (21a)$$

$$G_b(\omega + i0) = \frac{1}{\omega - \lambda_0 - \Sigma_b(\omega + i0)}, \quad (21b)$$

where the (finite) energy shift λ_0 is determined by fixing the local charge Q ,⁸

$$\begin{aligned} \lim_{\lambda \rightarrow \infty} e^{\beta\lambda} \left\langle \sum_{\sigma} f_{\sigma}^{\dagger} f_{\sigma} + b^{\dagger} b \right\rangle_G \\ = \int d\omega e^{-\beta\omega} \left[\sum_{\sigma} A_{f\sigma}(\omega) + A_b(\omega) \right] = 1. \end{aligned} \quad (22)$$

Here the subscript G specifies an expectation value in the grand canonical ensemble and $A_f(\omega) = -(1/\pi) \text{Im} G_f(\omega + i0)$, etc.

The remaining self-energies Σ_c and Σ_h contain one pseudoparticle loop each and are therefore $\propto e^{-\beta\lambda}$. The projected expectation value of any operator that vanishes in the $Q=0$ subspace is then given by²³

$$\langle A \rangle = \lim_{\lambda \rightarrow \infty} \frac{\langle A \rangle_G}{\langle Q \rangle_G} = \lim_{\lambda \rightarrow \infty} e^{\beta\lambda} \langle A \rangle_G \quad (23)$$

using Eq. (22). It follows that

$$\begin{aligned} \Sigma_{c,\sigma}(\omega+i0) = & V^2 \int d\xi e^{-\beta\xi} [G_{f\sigma}(\xi+\omega+i0)A_b(\xi) \\ & - A_{f\sigma}(\xi)G_b(\xi-\omega-i0)]. \end{aligned} \quad (24)$$

With the help of Eq. (16) we find the imaginary part of the impurity Green's function in the compact form

$$\text{Im } G_{imp,\sigma}(\omega+i0) = -\frac{\pi}{f(-\omega)} \int d\xi e^{-\beta\xi} A_{f\sigma}(\xi+\omega)A_b(\xi). \quad (25)$$

From Eq. (19e) one finds after analytical continuation and projection

$$\begin{aligned} \Sigma_{h\alpha}(\omega+i0) = & \frac{I^2}{4} \sum_{\sigma,\sigma'} \tau_{\sigma\sigma'}^\alpha \tau_{\sigma'\sigma}^\alpha \int d\xi e^{-\beta\xi} \\ & \times [A_{f\sigma}(\xi)G_{f\sigma'}(\xi+\omega+i0) \\ & + G_{f\sigma}(\xi-\omega-i0)A_{f\sigma'}(\xi)]. \end{aligned} \quad (26)$$

The impurity susceptibility is obtained from Eqs. (17) and (26) as

$$\begin{aligned} \text{Im } \chi_{imp,\alpha}(\omega+i0) = & \frac{\pi}{4n(\omega)} \sum_{\sigma,\sigma'} \tau_{\sigma\sigma'}^\alpha \tau_{\sigma'\sigma}^\alpha \\ & \times \int d\xi e^{-\beta\xi} A_{f\sigma}(\xi-\omega)A_{f\sigma'}(\xi). \end{aligned} \quad (27)$$

Equations (7)–(13), together with the ‘‘impurity solver,’’ Eqs. (18), (19a)–(19c), (22), (25), and (27) have been solved self-consistently. Starting with given initial values of the fermionic and bosonic bath and pseudoparticle spectral functions $A_c(\xi)$ and $D_h(\xi)$, the first approximation to the pair of impurity Green's functions G_{loc} and χ_{loc} as well as the pseudoparticle spectral functions is determined. Using the identities

$$G_{loc} = \sum_{\mathbf{k}} \frac{1}{G_{loc}^{-1} + V^2 G_c - \epsilon_{\mathbf{k}}}, \quad (28)$$

$$\chi_{loc} = \sum_{\mathbf{q}} \frac{1}{\chi_{loc}^{-1} - I^2 G_h + J_{\mathbf{q}}}, \quad (29)$$

which follow from Eqs. (2), (7), (8), (10) and (3), (7), (9), (11), the new bath spectral functions $A_c = (-1/\pi)\text{Im } V^2 G_c$ and $D_h = (-1/\pi)\text{Im } I^2 G_h$ may be deduced. With these and the updated pseudoparticle Green's functions one determines new G_{loc} , χ_{loc} , G_f , and G_b with the help of the impurity solver. The iteration is continued until convergence is found to the desired level. This process is found to converge well in the temperature regime $T \geq 0.04t$ using a nearest-neighbor tight-binding model, where t is the hopping amplitude. At lower T a solution could not be found anymore. In the following we will present the results of the numerical evaluation before discussing in detail the reasons for the breakdown of the solution in the low-temperature domain.

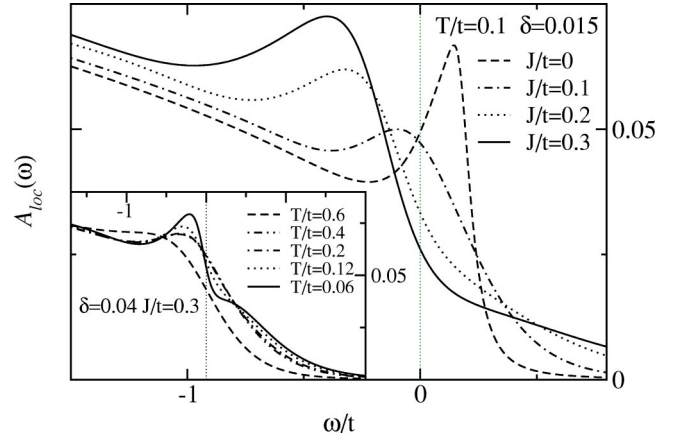


FIG. 2. The local spectral function plotted vs frequency for four different $J/t=0, 0.1, 0.2,$ and 0.3 and $T=0.1t$ for doping level of $\delta=0.015$. The evolution of the pseudogap of width J is clearly visible. The zero of energy is set at the chemical potential μ . The inset shows temperature dependence of the local spectral function at the doping level 4% and for $J=0.3t$.

IV. RESULTS

A. Local spectral function: Pseudogap and non-Fermi-liquid physics

The most striking result of our work is the appearance of a pseudogap in the local electron spectral function $A_{loc}(\omega)$ at small hole doping and low temperatures. For the purpose of this paper we define the pseudogap as a pronounced reduction of the density of states at the Fermi energy. Figure 2 shows how the pseudogap starts to form when the exchange interaction J is switched on, for $\delta=0.015$ and $T=0.1t$. In the limiting case of $J=0$, corresponding to the Hubbard model in the limit $U \rightarrow \infty$, $A_{loc}(\omega)$ is characterized by a broad maximum below the Fermi level ($\omega=0$), interpreted as the lower Hubbard band, and a narrow peak (‘‘quasiparticle peak’’) above $\omega=0$. As J is switched on, the quasiparticle peak disappears rapidly and the weight under it appears to be shifted a distance $\sim J$ below the Fermi level, forming a peak-dip-hump structure. The width of the pseudogap appears to scale with J . At the same time the spectral function develops a tail above $\omega=0$ reaching far ($\sim t$) above the bare band edge. It is instructive to observe how the pseudogap disappears for a given $J=0.3t$ at $T=0.06t$ with increasing doping level (Fig. 3). The pseudogap vanishes and the quasiparticle peak begins to appear at dopings above $\delta \approx 0.1$. In the inset of Fig. 2 the temperature dependence of the pseudogap feature is shown at $\delta=0.04$. Note that $A_{loc}(\omega=0)$ is weakly affected, as the main effect of temperature is a smearing of the pseudogap structure. We note in passing that the bulk of the spectral weight in the lower Hubbard band is shifted rigidly with the chemical potential and only a section of width $\sim 4 \max(J, \delta t)$ at the chemical potential is changing with the doping.

The formation of the pseudogap at a low doping $\delta=0.04$ and fixed $J=0.3t$ as the temperature is lowered from $T=2J$ down to $T=0.2J$ is shown in the inset of Fig. 2. In order to quantify the appearance of the pseudogap for given

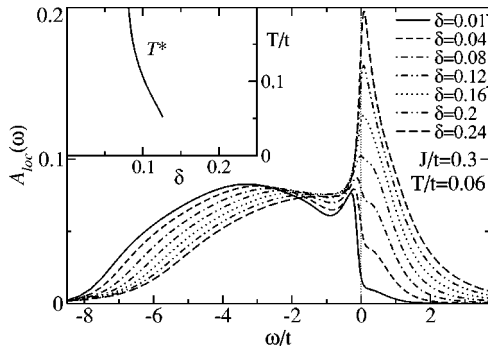


FIG. 3. The local spectral function plotted vs frequency for $T = 0.06t$ and $J/t = 0.3$ for various hole-doping concentrations δ . The inset shows the characteristic temperature T^* where the pseudogap opens (for the definition see the main text).

δ as a function of T one may define the temperature T^* at which the curvature of $A_{loc}(\omega)$ at $\omega=0$ changes sign from negative to positive values as T is lowered. In the inset of Fig. 3 the T^* values determined in this way are plotted versus δ . T^* is seen to drop rapidly with δ , tending to zero at $\delta \sim 0.15$. These results are reminiscent of what is seen in ARPES experiments on high T_c superconductors.¹¹

How is the pseudogap generated? The clue to this question lies in the behavior of the effective chemical potential $\mu_{eff} = \mu - \text{Re} \Sigma(0)$, as a function of doping. In Fig. 4, μ_{eff} is shown at a low temperature $T = 0.06t$, in comparison with the effective chemical potential μ_0 of a Fermi liquid (which due to Luttinger's theorem and the momentum independence of Σ coincides with the chemical potential of a noninteracting system). At doping levels $\delta \geq 0.2$ one finds that μ_{eff} coincides namely with μ_0 , a necessary condition for Fermi liquid behavior. Upon lowering the doping concentration, μ_{eff} is seen to grow until at $\delta \approx 0.02$ the upper edge of the bare band is reached (the zero of energy is fixed at the center of the tight-binding band). In fact μ_{eff} moves above the bare

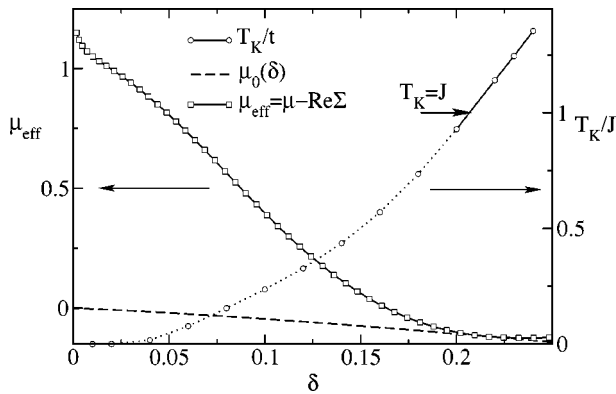


FIG. 4. Open squares mark the effective chemical potential μ_{eff} in units of $4t$ vs doping for $J = 0.3t$ and $T = 0.06t$ (left scale). The dashed line shows the effective chemical potential μ_0 of a Fermi liquid at $T = 0$ (see text). Open circles mark the estimation for the Kondo temperature T_K vs doping as calculated from Eq. (31) (right scale). The arrow marks the position where T_K is equal to J . Only in the regime where T_K is larger than J does the solution show the onset of a Fermi liquid phase.

band, signaling the availability of states even above the latter. By contrast, the validity of Luttinger's theorem would require that the chemical potential be located in the center of the band, approaching $\mu_0 = 0$ in the limit $\delta \rightarrow 0$. The fact that μ_{eff} is moving up towards the upper band edge for $\delta \rightarrow 0$ is a strong and unequivocal signal of non-Fermi-liquid behavior—it is only possible for a highly incoherent metal with a large $\text{Im} \Sigma$. It is interesting to recall that in DMFT for the Hubbard model (which in the limit $U \rightarrow \infty$ is identical to the t - J model for $J \rightarrow 0$) one finds Fermi liquid behavior at low temperatures and $\mu_{eff} = \mu_0$. Even at not so low temperatures ($T \geq 0.06t$) for $J = 0$, μ_{eff} follows μ_0 except at rather low doping values $\delta \leq 0.05$, where a strong temperature dependence appears.

That indeed strong inelastic scattering drives the effective chemical potential out of the band and that this induces a reduction of the density of states is shown in Appendix B for a toy model describing the pseudogap formation in a doped band insulator in the presence of strong inelastic scattering. For sufficiently low δ , μ_{eff} moves beyond the bare band edge as the scattering strength—i.e. $|\text{Im} \Sigma|$ —is increased. As a consequence, the local spectral function at the Fermi level drops dramatically. Also for a doped Mott insulator and a flat density of states, we show explicitly in Appendix B that a pseudogap is generated if μ_{eff} is moving from the center of the lower Hubbard band to or above the upper band edge.

Similar behavior has been found in Refs. 16 and 17 for the Hubbard model at intermediate coupling. In Ref. 16 the dynamical cluster approximation involving up to 64 sites was employed and the mean-field equations were solved by QMC simulation and the maximum entropy method, to effect the analytical continuation from imaginary to real frequencies. Maier *et al.*¹⁶ interpreted the pseudogap found in their spectra as generated by finite-range antiferromagnetic correlations on the cluster or as RVB physics. Note that in our approach *finite*-range AF correlations and the formation of intersite singlets are not included as magnetic fluctuations on neighboring sites are treated as uncorrelated. Since the results of Ref. 16 are so similar to ours—including violations of Luttinger's theorem in the relevant T range—we suggest that their pseudogap is created by the same mechanism we identify as being responsible for our pseudogap: incoherent fluctuations (see above). In their approach the self-energy and therefore the pseudogap show a pronounced momentum dependence not captured by our approximation. Within the picture sketched above, a \mathbf{k} dependence of $\Sigma_{\mathbf{k}}$ would give rise to a momentum dependence of the “effective chemical potential” $\mu_{eff} = \mu - \text{Re} \Sigma_{\mathbf{k}}$ and therefore of the pseudogap. Stanescu and Phillips¹⁷ used a two-site cluster approach to derive nonlocal DMFT equations. The quantum impurity model was solved by an adaptation of the noncrossing approximation. Again the results for the spectral functions are similar to ours. The authors claim that an effective low-energy model cannot be defined, as low- and high-energy sectors are mixed in a dynamical way. We do not see any reason for such an unusual situation, either from their paper or from outside arguments. Rather, in the limit $U \gg t$ or, more precisely, if U is strong enough to generate a Mott gap, the separation of the lower and upper Hubbard bands is well

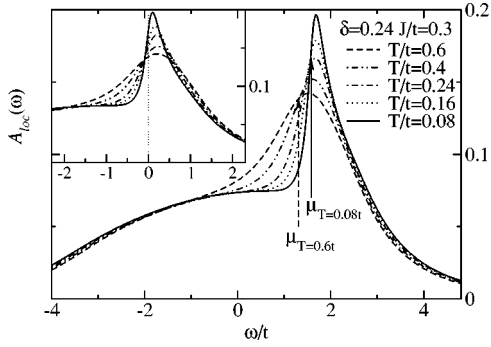


FIG. 5. Temperature evolution of local spectral function for doping level $\delta=0.24$. In the main panel, the arrows show the position of the chemical potential while the inset shows spectra with the chemical potential fixed at $\omega=0$. The evolution of broad quasiparticle peak above the Fermi level is clearly visible.

defined, and a projection onto the lower band is justified. In Ref. 17 the appearance of the pseudogap is attributed to short-range (nearest-neighbor) correlations, limiting the phase space for low-energy excitations. These correlations are identified as orbital ring currents flowing between three adjacent sites. Since such effects are not included in our calculation and we nonetheless find a pseudogap and a violation of Luttinger's theorem, very similar to Ref. 17, we conclude that the interpretation given in Ref. 17 (as sketched above) is not conclusive.

We conclude that the behavior found in our scheme for low doping—namely, pseudogap and non-Fermi-liquid physics—is a generic feature of an incoherent metal. We have found this incoherent state to be quite robust, e.g., against changes in band structure. It is worth mentioning that Parcollet and Georges²⁴ recently studied a t - J model with random J , which is equivalent to our EDMFT equations for the Bethe lattice. They did not find indications for a pseudogap. We believe the reason is that they employ slave-boson mean-field theory and, thereby, miss the incoherent part of the spectral function. A similar spin model has been considered before by Sachdev and Ye.²⁵

At larger dopings the solution shows the onset of a Fermi liquid phase, which we now proceed to discuss. First we show in Fig. 5 the local spectral function at $\delta=0.24$ and $J=0.3t$. With increasing temperature the quasiparticle peak broadens and the chemical potential shifts to lower energies. The value of $A(\omega)$ at the Fermi level increases with falling temperature and tends to a limiting value as $T \rightarrow 0$.

At large doping the exchange interaction J is unimportant and the EDMFT model reduces to an Anderson impurity model. We may estimate the hybridization width Γ of this model from the density of states of the fermionic bath at the Fermi level ($\omega=0$):

$$\Gamma = \pi A_c(\omega=0). \quad (30)$$

The energy of the local orbitals E_d , according to Eq. (6), is given by the chemical potential $E_d = -\mu$. An estimate of the Kondo temperature is obtained from the conventional expression $T_K = \sqrt{D\Gamma} \exp(\pi E_d/2\Gamma)$ as

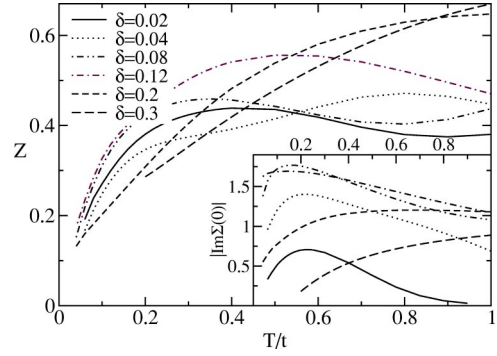


FIG. 6. Quasiparticle renormalization amplitude Z plotted vs temperature for various doping concentrations. The inset shows the imaginary part of the self-energy at zero frequency as a function of temperature.

$$T_K = \sqrt{D\pi A_c(0)} \exp\left(-\frac{\mu}{2A_c(0)}\right). \quad (31)$$

Figure 4 shows T_K/t as a function of δ for the low temperature $T=0.1t$, using $D=2t$. The Kondo temperature is seen to fall strongly with decreasing δ even at the highest value $\delta=0.24$ and approaches zero rapidly in the pseudogap regime. The value where $T_K=J$ is indicated. In the regime $T_K \lesssim J$ (dotted line) one expects the exchange interaction to be of increasing importance, such that the interpretation in terms of an Anderson impurity model loses its meaning.

In the Fermi liquid regime the imaginary part of the self-energy of G_{loc} is expected to vary as

$$\text{Im} \Sigma(\omega - i0) \sim t[\omega^2 + (\pi T)^2]/T_K^2, \quad (32)$$

where the Kondo temperature T_K plays the role of the renormalized Fermi energy. The quadratic dependence is expected to hold for $\omega, T \ll T_K$. The inset of Fig. 6 shows $\text{Im} \Sigma(0)$ as a function of T for doping levels from $\delta=0.3$ down to 0.01. A limiting quadratic temperature dependence is not seen since the lowest temperature reached in our evaluation is above T_K (or, for $\delta > 0.2$, only slightly below T_K).

However, for $\delta=0.3$ behavior consistent with Fermi liquid theory would smoothly match the results shown. For smaller doping, in particular around $\delta \sim 0.1$, $\text{Im} \Sigma$ at $T \sim 0.03t$ is so large that it is impossible to connect this behavior smoothly with a Fermi liquid behavior below $T_K \approx 0.1t$. At still smaller δ , $\text{Im} \Sigma$ is seen to decrease with doping, due to the formation of the pseudogap.

As a further indication of Fermi liquid behavior we evaluate the quasiparticle weight factor Z defined as

$$Z = \left(1 - \frac{\partial \text{Re} \Sigma}{\partial \omega}\right)_{\omega=0}^{-1}. \quad (33)$$

Figure 6 shows Z as a function of temperature for $\delta = 0.02$ – 0.3 . A finite quasiparticle weight in the limit $T \rightarrow 0$ would signal Fermi liquid behavior. It is seen that only for the highest doping levels $\delta=0.3$ and 0.24 would an extrapolation to $T=0$ give a finite value. For smaller values of δ the Z factor appears to drop rapidly with decreasing temperature, possibly extrapolating to zero.

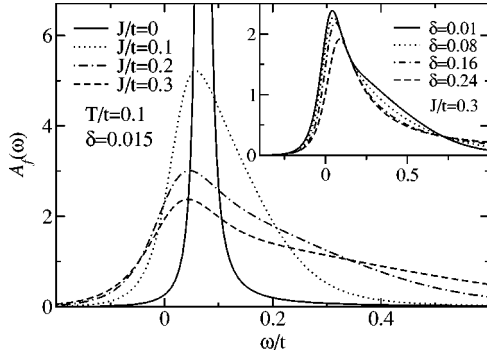


FIG. 7. The pseudofermion spectral function plotted vs frequency for four different values of J . The inset shows the evolution of spectra by doping the system at constant $J=0.3t$.

B. Pseudoparticle spectral functions

The pseudofermion spectral function $A_f(\omega)$ at $\delta=0.015$ and $T=0.1t$ is plotted versus ω/t in Fig. 7, for values of J/t from 0 to 0.3. While at $J=0$ $A_f(\omega)$ is characterized by a narrow peak at a frequency $\omega \sim T$ and of width $\sim T$, increasing J leads to a rapid asymmetric broadening of the peak, of width $\Delta\omega \sim J$. Although in the limit $T \rightarrow 0$ for general reasons one expects $A_f(\omega)$ [and also $A_b(\omega)$] to acquire power-law divergent behavior at the threshold $\omega=0$,²⁶ the temperature $T=0.1t$ is too high to show the asymptotic behavior. At large doping, $\delta > 0.2$, when the Kondo temperature T_K as defined in Eq. (31) is larger than J , $A_f(\omega)$ is hardly affected by J . The doping dependence of $A_f(\omega)$ at $J=0.3t$, as shown in the inset of Fig. 7, is weak. The characteristic energy scale is $\max(J, T_K) \approx J$ up to the highest doping of $\delta=0.24$ and, hence, is independent of δ .

The pseudoboson spectral function shown in Fig. 8 is roughly speaking a mirror image of the lower Hubbard band. As J is switched on spectral weight is pushed from below the threshold at $\omega=0$ and from the far end of the Hubbard band into a peak at $\omega \sim J$, emulating the peak-dip-hump structure in $A_{loc}(\omega)$ in the pseudogap regime.

Both in the case of $J=0$ and for $\delta > 0.2$ a sharp quasiparticle peak is observed to form in $A_b(\omega)$ at $\omega=0$. The peak is suppressed at temperatures $T \gg T_K$, which is why it is not seen in Fig. 8. In contrast to $A_f(\omega)$, $A_b(\omega)$ is strongly doping dependent, as shown in Fig. 8. At the moderately low

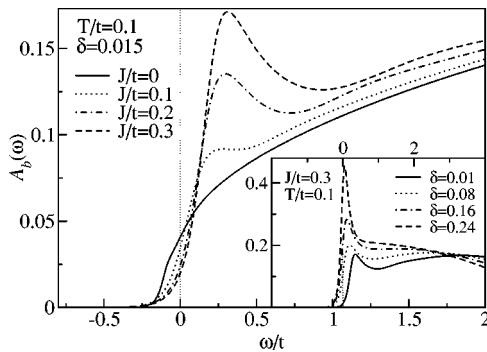


FIG. 8. The pseudoboson spectral function for the same parameters as used in Fig. 7.

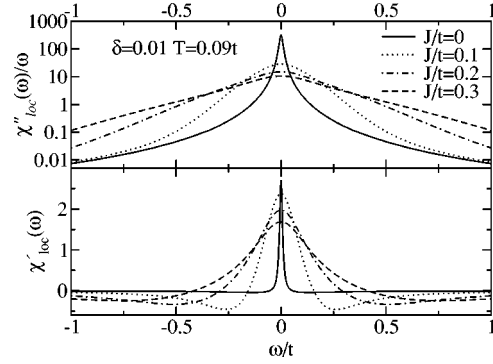


FIG. 9. The local dynamical spin susceptibility plotted vs frequency for four different J/t and doping concentration $\delta=0.01$.

temperature of $T=0.1t$ and for $J=0.3t$, the pseudogap feature at small δ is seen to smoothly cross over to the quasiparticle peak at large doping.

C. Dynamical spin susceptibility

The dynamical spin susceptibility is expected to reveal how the character of spin fluctuations depends on doping and exchange coupling constant J . In Fig. 9 the imaginary part of $\chi_{loc}(\omega)/\omega$ is shown at low doping $\delta=0.01$ and low temperature $T=0.09t$ for various values of J/t ranging from 0 to 0.3. As J is increased, the peak of $\text{Im}(\omega)\chi/\omega$ broadens and the width is seen to be given by $\Delta\omega \approx J$. The real part $\text{Re}\chi(\omega=0) = \chi'(0)$ decreases with J as shown in Fig. 9. However, there is no trace of a pseudogap in $\text{Im}\chi_{loc}(\omega)$. The pseudogap reveals itself in the spectrum of the self-energy $M(\omega)$ of magnetic excitations, as shown in Fig. 10, where $\text{Im}M(\omega) = M''(\omega)$ is observed to develop a gap for $\omega \lesssim J$. As analyzed in Sec. V, the pseudogap is caused by large values of $\chi'(\omega)$, which force a redistribution of spectral weight in $M''(\omega)$ by way of the self-consistent feedback of $\chi'(\omega)$ into $M''(\omega)$. In Fig. 11, the momentum-resolved spin excitation spectrum $\chi_q''(\omega)/\omega$ is shown for $J=0.3t$, $\delta=0.01$, and $T=0.1t$. Whereas a pronounced gap exists at q values away from the antiferromagnetic wave vector $Q = (\pi, \pi)$, near Q the gap is filled in. This is due to the fact that in the region of \mathbf{q} space around \mathbf{Q} not only is $M''(\omega)$

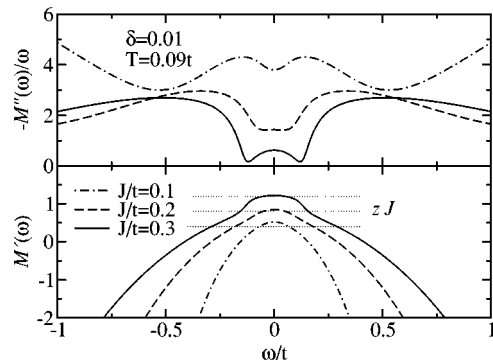


FIG. 10. The spin self-energy $M(\omega)$ plotted vs frequency for four different J/t . The horizontal dotted lines mark the value zJ , where $z=4$ is the coordination number.

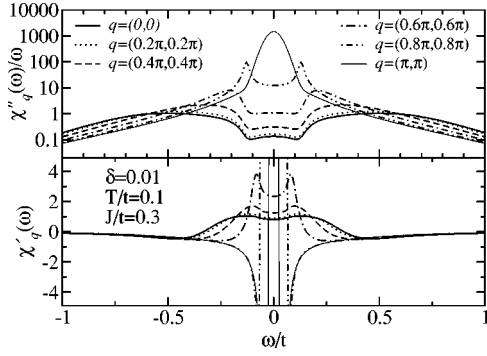


FIG. 11. The momentum-dependent spin susceptibility along the $(0,0) - (\pi,\pi)$ axis plotted as a function of frequency for doping concentration $\delta=0.01$ and temperature $T=0.1t$.

small for $\omega \leq J$, but also the real part of the denominator of $\chi_q(\omega)$ vanishes, as $M'(\omega) + J_q \rightarrow 0$ for $q \rightarrow Q$ and as the transition to the antiferromagnetically ordered state is approached. Consequently, the ratio $M''(\omega)/|\chi_q(\omega)|^2$ develops pronounced peaks at $|\omega| \sim J$ rather than a pseudogap. In the local susceptibility the contribution from $q \approx Q$ tends to fill in the pseudogap, which is therefore not discernible in Fig. 9. The effect of approaching the ordered state is also observed in the real part of $\chi_q(\omega)$, shown in Fig. 11. The static q -dependent susceptibility $\chi_q(0)$ is seen to grow by two orders of magnitude as q is varied from $q=0$ to $q=Q$. This behavior reflects the effect of a large spin correlation length ξ , defined through

$$\chi_q(0) = \frac{2}{zJ} \frac{1}{\xi^{-2} + (\mathbf{q} - \mathbf{Q})^2}, \quad (34)$$

for $\mathbf{q} \approx \mathbf{Q}$ ($z=4$ is the coordination number and length is measured in units of the lattice constant). In Fig. 12 the inverse correlation length is plotted versus T/t for $J=0.3t$ and for various doping levels. For comparison, the theoretical result for the Heisenberg model (two-loop order RG of the nonlinear σ model) given in Refs. 2 and 27 (limit $\delta=0$) is shown as well. It appears to connect smoothly to the curve for $\delta=0.02$. Figure 12 also serves to show that the numerical solution ceases to exist at $\chi_Q(0) \geq 10^2$, as will be discussed in Sec. V.

D. Spectral functions of the fermionic and bosonic baths

The spectral function $A_c(\omega)$ of the fermionic bath is shown for $J=0.3t$ and at $T=0.1t$ in Fig. 13. The imposed self-consistency of the EDMFT equations has led to a drastic renormalization of the structureless tight-binding density of states. In fact $A_c(\omega)$ reflects the structure seen in $A_{loc}(\omega)$ to a large degree: on the one hand, the quasiparticle peak at large doping and, on the other, the pseudogap at small δ . For comparison we show $A_{loc}(\omega)$ in Fig. 13 as well.

A similar trend is seen in the case of the spectral function of the bosonic bath $D_h(\omega)$, as is apparent from Fig. 14. Here we also see from the comparison with $\chi''_{loc}(\omega)$ a large degree of similarity.

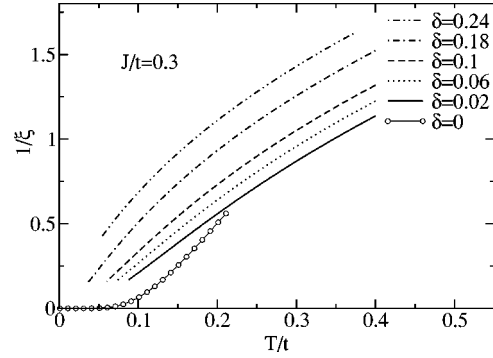


FIG. 12. The inverse of dynamic correlation length plotted as a function of temperature for various doping levels. The curve for $\delta=0$ is taken from Ref. 27 and corresponds to the two-dimensional Heisenberg model.

The total weight under the spectral functions $A_c(\omega)$ and $D_h(\omega)$ is equal to the squares of the coupling constants V^2 and I^2 , respectively. As shown in Appendix C, the coupling constant V^2 is fixed by sum rules and is given by

$$V^2 = 2t^2(1 + \delta). \quad (35)$$

In contrast, a similarly simple relation does not hold for I^2 . However, I^2 may be related to χ_{loc} and M as follows:

$$I^2 = \int_0^\infty \frac{d\omega}{\pi} \text{Im}[M(\omega - i0) - \chi_{loc}^{-1}(\omega - i0)]. \quad (36)$$

It turns out that the numerical evaluation yields

$$I^2 \approx 2J^2(1 - \delta). \quad (37)$$

The first moment of the eigenfrequencies ω_q of the bosonic bath is given by the f -sum rule

$$\bar{\omega}_q \equiv \sum_q \omega_q = \frac{\langle \epsilon^2 \rangle}{2I^2} \int_{-\infty}^\infty \frac{d\omega}{\pi} \omega \chi''_{loc}(\omega), \quad (38)$$

where $\langle \epsilon^2 \rangle = \int d\epsilon \epsilon^2 N_J(\epsilon)$ and $N_J(\epsilon)$ is the density of states (DOS) of $J_{\mathbf{q}}$.

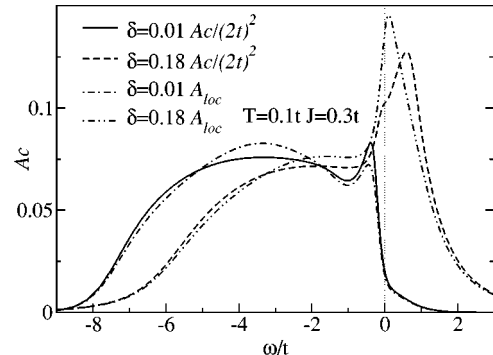


FIG. 13. The fermionic bath spectral function A_c for two different doping levels $\delta=0.01$ and $\delta=0.18$ at $J=0.3t$ and $T=0.1t$. The local spectral function is also shown for comparison.

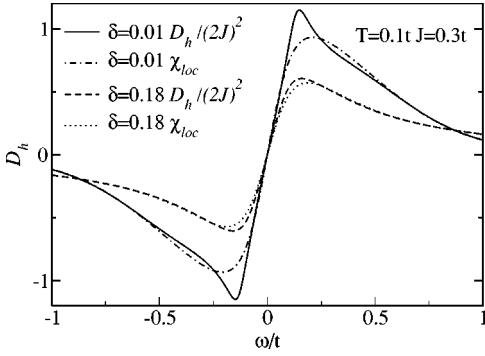


FIG. 14. The bosonic bath spectral function D_h for two different doping levels $\delta=0.01$ and $\delta=0.18$ at $J=0.3t$ and $T=0.1t$. For comparison, the local dynamic spin susceptibility is also shown.

E. Thermodynamic properties

The thermodynamic potential Ω within EDMFT can be expressed in terms of the impurity free energy Ω_{imp} and contributions from the fermionic and bosonic baths:

$$\Omega = \Omega_{imp} + k_B T \sum_{i\omega} \left\{ \sum_{\mathbf{k},\sigma} \ln[G_{\mathbf{k}\sigma}(i\omega)/G_{loc,\sigma}(i\omega)] + \frac{1}{2} \sum_{\mathbf{q},\alpha} \ln[\chi_{\mathbf{q}}^{\alpha\alpha}(i\omega)/\chi_{loc}^{\alpha\alpha}(i\omega)] \right\} e^{i\omega 0^+}. \quad (39)$$

Performing the analytical continuation from imaginary frequencies to the real axis and expressing the momentum summations as energy integrals, Eq. (39) may be written as

$$\Omega = \Omega_{imp} + \frac{1}{\pi} \int d\epsilon D(\epsilon) \times \text{Im} \left\{ 2 \int d\omega f(\omega) \ln[G_{loc}(\omega)[\omega + \mu - \Sigma(\omega) - \epsilon]] + \frac{3}{2} \int d\omega n(\omega) \ln\left[\chi_{loc}(\omega) \left(M(\omega) + \frac{J}{t} \epsilon\right)\right] \right\}. \quad (40)$$

The impurity free energy is given by the shift of the chemical potential,⁸ λ_0 , defined by Eq. (22):

$$\Omega_{imp} = \lambda_0. \quad (41)$$

The entropy $S = -(\partial\Omega/\partial T)_\mu$ as a function of doping concentration δ for various temperatures is shown in Fig. 15. Even at the low temperature $T=0.1t$, S is seen to be rather large ($\sim 0.5 \ln 2$), an indication for strong correlations and a rather incoherent state. The entropy of a noninteracting system at the same density would be about an order of magnitude smaller. The overall magnitude of S compares well with both the results of exact diagonalization²⁸ for a small system and experimental data for $\text{La}_{2-x}\text{Sr}_x\text{CuO}_4$ (Ref. 29). The calculated entropy shares the trend that it is reduced both at large doping, when the system crosses over to a Fermi liquid, and at smaller doping in the pseudogap phase. The quenching of the magnetic fluctuations by the incipient magnetic order as the antiferromagnetic Mott insulator is approached

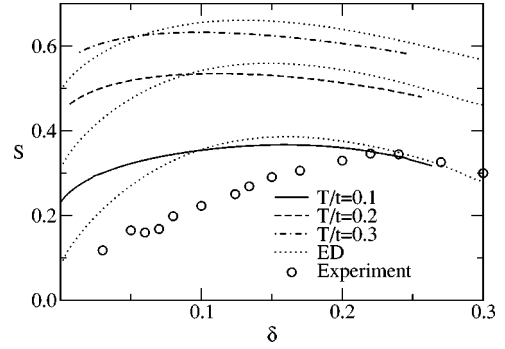


FIG. 15. Entropy per site as a function of doping δ at various temperatures. Exact diagonalization results (Ref. 28) for the same temperatures are denoted by dotted lines while the open circles correspond to the experimental data (Ref. 29) on $\text{La}_{2-x}\text{Sr}_x\text{CuO}_4$.

for $\delta \rightarrow 0$ is qualitatively reproduced (note that for $J=0$, S increases as $\delta \rightarrow 0$, and this behavior is obtained in DMFT calculations of the Hubbard model). Not only the doping dependence but also the temperature dependence compares well with exact diagonalization results as shown in Fig. 16.

Another thermodynamic quantity of interest is the particle density n , given by

$$n = 1 - \delta = - \left(\frac{\partial \Omega}{\partial \mu} \right)_T. \quad (42)$$

In Fig. 17 the doping δ is plotted versus μ at $T=0.1t$. As expected, δ varies monotonically with μ , with positive curvature.

The particle density may also be obtained from the local Green's function as $n = 2G_{loc,\sigma}(\tau=0^+)$. The resulting values of n are indistinguishable from those calculated by differentiating Ω , which provides a check for numerical accuracy within our conserving approximation.

F. Transport properties

The calculation of transport properties in EDMFT is facilitated by the observation that a momentum independent self-energy leads to a local current vertex function (in other words, the nonlocal parts vanish in the limit dimension $d \rightarrow \infty$) (Refs. 30–32). The optical conductivity is therefore given by the single-particle Green's function as

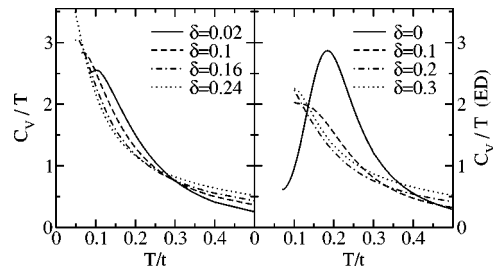


FIG. 16. Specific heat coefficient vs temperature for various doping concentrations. In the right panel we show results obtained by the exact diagonalization (Ref. 28).

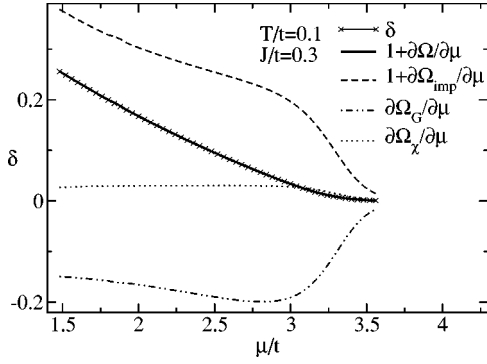


FIG. 17. Solid line: derivative of the thermodynamic potential with respect to chemical potential $1 + (\partial\Omega/\partial\mu)_T$ (or equivalently doping vs chemical potential). The contributions from three different parts of the thermodynamic potential—impurity, electron Green's function [second term in Eq. (40)], and spin susceptibility part [last term in Eq. (40)]—are shown separately.

$$\sigma_{xx}(i\omega) = \frac{e^2}{\omega} k_B T \sum_{i\omega'} \sum_{\mathbf{k}\sigma} (v_{\mathbf{k}}^x)^2 G_{\mathbf{k}}(i\omega') G_{\mathbf{k}}(i\omega' + i\omega), \quad (43)$$

where $v_{\mathbf{k}}^x = 2t \sin k_x$ is the bare current vertex. Using the fact that $G_{\mathbf{k}}$ depends on \mathbf{k} only through $\epsilon_{\mathbf{k}}$ [see Eqs. (2) and (4)] and performing the analytical continuation to the real frequency axis one finds

$$\begin{aligned} \text{Re } \sigma_{xx}(\omega + i\delta) &= 2\pi e^2 \int d\epsilon \Phi_{xx}(\epsilon) \\ &\times \int d\omega' \frac{f(\omega') - f(\omega' + \omega)}{\omega} \\ &\times A(\epsilon, \omega') A(\epsilon, \omega' + \omega), \end{aligned} \quad (44)$$

where

$$\Phi_{xx}(\epsilon) = \sum_{\mathbf{k}} (v_{\mathbf{k}}^x)^2 \delta(\epsilon - \epsilon_{\mathbf{k}}) \quad (45)$$

and $A(\epsilon_k, \omega) = (1/\pi) \text{Im } G_{\mathbf{k}}(\omega - i\delta)$.

Similarly, the off-diagonal or Hall conductivity in the presence of a magnetic field \mathcal{B} perpendicular to the plane takes the form^{33–35}

$$\sigma_{xy} = \frac{4\pi^2 e^3}{3} \mathcal{B} \int d\epsilon \Phi_{xy}(\epsilon) \int d\omega \left(-\frac{\partial f}{\partial \omega} \right) [A(\epsilon, \omega)]^3, \quad (46)$$

where

$$\Phi_{xy}(\epsilon) = \sum_{\mathbf{k}} \det(\mathbf{k}) \delta(\epsilon - \epsilon_{\mathbf{k}}) \quad (47)$$

and

$$\det(\mathbf{k}) = \begin{vmatrix} (\epsilon_k^x)^2 & \epsilon_k^{xy} \\ \epsilon_k^x \epsilon_k^y & (\epsilon_k^y)^2 \end{vmatrix}, \quad \epsilon_k^\alpha = \frac{\partial \epsilon_{\mathbf{k}}}{\partial k_\alpha}, \quad \epsilon_k^{\alpha\beta} = \frac{\partial^2 \epsilon_{\mathbf{k}}}{\partial k_\alpha \partial k_\beta}. \quad (48)$$

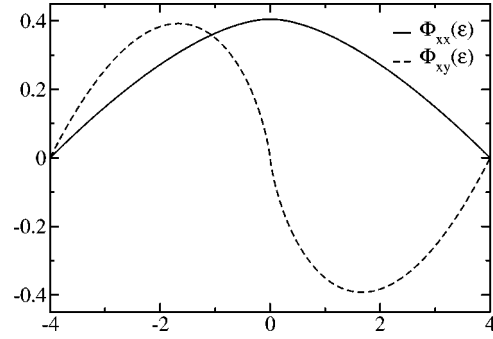


FIG. 18. The weighting functions for the two-dimensional square lattice can be expressed by elementary functions as $\Phi_{xx}(x) = (2t/\pi^2)[2|x|E(1-1/x^2) + 2K(1-1/x^2) - 2\Pi(1-1/|x|, 1-1/x^2)]$ and $\Phi_{xy}(x) = 2(2t/\pi)^2[x^2E(1-1/x^2) - K(1-1/x^2)]\text{sgn}(x)$. Here, $K(x)$, $E(x)$, and $\Pi(x)$ are complete elliptic integrals of the first, second, and third kinds and $x = \epsilon/(4t)$.

The weight factors Φ_{xx} and Φ_{xy} are shown in Fig. 18. One observes that for the simple 2D tight-binding lattice, Φ_{xx} is an even function of energy, while Φ_{xy} is an odd function of energy.

The Hall coefficient \mathcal{R}_H is defined as

$$\mathcal{R}_H = \frac{\sigma_{xy}}{\sigma_{xx}^2 \mathcal{B}}. \quad (49)$$

For orientation it is useful to discuss the limit of low temperatures, assuming $\text{Im } \Sigma(\omega) \rightarrow 0$ at $\omega \rightarrow 0$ and $A(\epsilon, \omega)$ sharply peaked as a function of ϵ at $\epsilon = \omega + \mu_{\text{eff}}$. One may then do the integrations on ϵ and ω in Eqs. (44) and (46), yielding

$$\sigma_{xx} \approx e^2 \frac{\Phi_{xx}(\mu_{\text{eff}})}{|\text{Im } \Sigma(0)|} \quad (50)$$

and

$$\mathcal{R}_H \approx \frac{1}{2e} \frac{\Phi_{xy}(\mu_{\text{eff}})}{[\Phi_{xx}(\mu_{\text{eff}})]^2}, \quad (51)$$

with $e = -|e|$. We observe that \mathcal{R}_H does not depend on $\text{Im } \Sigma$ in this limit. In the Fermi liquid regime $\mu_{\text{eff}} = \mu_0 < 0$, and consequently $\Phi_{xy}(\mu_0) > 0$, leading to a negative $\mathcal{R}_H < 0$.

By contrast, in the incoherent regime of the t - J model μ_{eff} is found to be positive, approaching the upper band edge for $\delta \rightarrow 0$ (see Fig. 4), since $\Phi_{xy}(\epsilon)$ is negative for positive ϵ and \mathcal{R}_H is seen to be positive (hole like). For $\delta > 0.17$, μ_{eff} changes sign and \mathcal{R}_H turns negative. For the nearest-neighbor tight-binding model and assuming a linear variation of μ_{eff} with δ , $\mu_{\text{eff}} = 4t(1 - C\delta)$, \mathcal{R}_H takes the simple form

$$\mathcal{R}_H \approx \frac{\pi}{2C} \frac{1}{|e|\delta}, \quad \delta \rightarrow 0, \quad C > 0. \quad (52)$$

Using in addition the result for a single hole in the half-filled band,³⁶ $\mathcal{R}_H = 1/|e|\delta$, one finds by comparison $C = \pi/2$. For the conductivity one obtains in a similar way

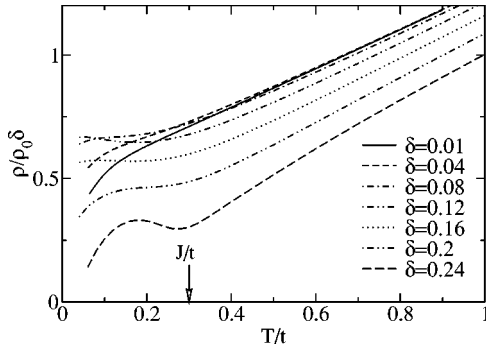


FIG. 19. T dependence of the resistivity multiplied by doping δ . The linear- T behavior for high T flattens for $\delta > 0.1$ at a temperature of the order of J . For $\delta < 0.1$ the resistivity drops in the regime where a pseudogap opens.

$$\sigma_{xx} \approx e^2 \frac{t\delta}{|\text{Im}\Sigma(0)|}, \quad \delta \rightarrow 0. \quad (53)$$

Although Eqs. (52) and (53) are in qualitative agreement with our numerical results, we emphasize that the assumption of small $\text{Im}\Sigma(0)$ is not justified in the incoherent regime. A large $\text{Im}\Sigma$ is actually necessary to obtain a μ_{eff} close to the band edge and therefore a positive sign of R_H .

We now present the numerical results. In Fig. 19 the scaled resistivity $\rho_{xx}\delta/\rho_0$, where $\rho_0 = \hbar/e^2$, is plotted versus temperature for values of δ ranging from 0.01 to 0.23. The curves form a narrow band, meaning that the scaling $\rho_{xx} \propto 1/\delta$ shown in Eq. (53) holds approximately [and $\text{Im}\Sigma(0)$ is a weak function of δ]. The values of the resistivity are rather high. In the pseudogap regime ($\delta \ll 0.1$) the resistivity tends to turn downward for decreasing temperature. By contrast, at higher dopings an upward curvature is observed, leading to a plateau at low T , before ρ begins to drop to lower values at still lower T . The plateau is likely to be an artifact of the NCA. The linear- T dependence of ρ at large temperatures has also been seen in DMFT calculations^{5,37} based on QMC simulations which do not include the effects of short-ranged magnetic fluctuations. The Hall coefficient is plotted in Fig. 20 versus temperature, for values of δ ranging from 0.01 to 0.23. For small doping $\delta < 0.16$, R_H is always positive, approaching the expected value³⁶ $1/(|e|\delta)$ in the limit $\delta \rightarrow 0, T$

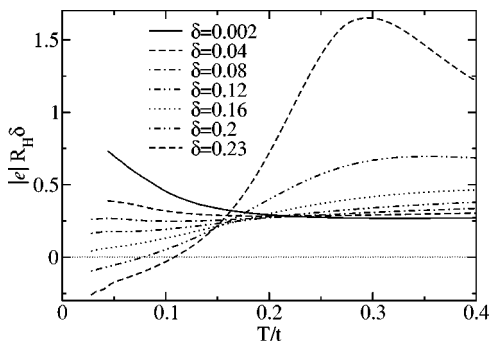


FIG. 20. T dependence of R_H for $J = 0.3t$. For small doping and $T \rightarrow 0$, R_H approaches the value $1/(|e|\delta)$ expected for a single hole in a t - J model.

$\rightarrow 0$. For doping levels $\delta \geq 0.16$, R_H is negative at low T , consistent with Eq. (51), and changes sign at higher T , similar to what is observed in experiment.⁴¹

V. INSTABILITY OF THE EDMFT SOLUTION DUE TO CRITICAL FLUCTUATIONS IN $d=2$

We will now investigate the question of why no solutions of the EDMFT equations exist for low temperatures and small dopings. Within the EDMFT of the t - J model long-range antiferromagnetic fluctuations are not taken into account in a proper way. As a consequence the local spin excitation spectrum $\chi''_{loc}(\omega) = \text{Im}\chi_{loc}(\omega - i0)$ keeps a simple Lorentzian-type shape. On the other hand, the static local susceptibility $\chi'_{loc}(0)$ (in two dimensions) diverges as $\ln\xi$ when the transition to the antiferromagnetically ordered state is approached and the spin correlation length $\xi \rightarrow \infty$. This in turn forces the slope of $\chi''_{loc}(\omega)$ in the limit $\omega \rightarrow 0$ to diverge as $\ln\xi$ as well. Within the effective impurity model of EDMFT a steep slope of $\chi''_{loc}(\omega)$ entails a large maximum of $\chi''_{loc}(\omega)$ at $\omega_{max} \lesssim J$, of value $\chi''_{loc}(\omega_{max}) \sim \chi'_{loc}(0)$. As will be shown below, a maximum value of $\chi''_{loc}(\omega_{max})$ larger than some critical value $\chi''_{loc,crit} = c/J$, where the constant c depends on the density of states $N_J(\epsilon)$ [see Eq. (54)], leads to an unphysical pole in $\chi_q(\omega)$ at $\omega = \omega_{max}$ and $q = q_{max}$. This in turn forces $\text{Im}M(\omega - i0)$ to change sign into an unphysical branch of the complex frequency plane. This is the point when a stable numerical solution cannot be found any longer.

To demonstrate this behavior explicitly we consider now a flat density of states of spin excitations,

$$N_J(\epsilon) = \sum_{\mathbf{q}} \delta(\epsilon - J_{\mathbf{q}}) = \frac{1}{8J} \theta(4J - |\epsilon|), \quad (54)$$

where the bandwidth $8J$ has been chosen to agree with that of the tight-binding model, $J_{\mathbf{q}} = 2J(\cos q_x + \cos q_y)$. The local susceptibility as defined by Eq. (9) may then be expressed analytically in terms of the self-energy $M(\omega)$:

$$\chi_{loc}(\omega - i0) = \frac{1}{8J} \ln \frac{4J + M(\omega - i0)}{-4J + M(\omega - i0)} = \chi' + i\chi''. \quad (55)$$

Inverting this relation one finds

$$M(\omega - i0) = 4J \frac{v+1}{v-1} = 4J \frac{|v|^2 - 1 - 2iv''}{|v-1|^2}, \quad (56)$$

where $v = \exp(8J\chi) = v' + iv''$. The imaginary part of v , given by

$$v'' = \exp(8J\chi') \sin(8J\chi''), \quad (57)$$

will change sign as $\chi''(\omega)$ increases with increasing ω , if $8J\chi'' \geq \pi$. By Eq. (56), this will lead to a sign change of $M''(\omega - i0)$ from negative (stable) to positive values. How can χ'' and M'' both be positive? This is possible since $\chi_q(\omega - i0)$ develops a pole in the physical domain, $-|J_{\mathbf{q}}| < 4J$, at finite $\omega = \omega_{max}$, giving a contribution to χ_{loc} with

the “right” sign. The instability occurs at finite frequency and thus is not easily interpreted as a physical phenomenon.

In the numerical treatment we found that a convergent solution cannot be obtained when the stability criterion

$$\chi''_{loc} < \frac{c}{J} \quad (58)$$

is violated. The constant c takes the value $\pi/8$ for the flat DOS and a value ≈ 0.3 for the tight-binding model.

We emphasize that this instability is not an artifact of the method of solution of the impurity model but is a generic feature of the EDMFT equations in two dimensions. In the following we argue that whenever the ground state at $T=0$ is ordered, the self-consistency scheme has to break down below some finite temperature. This argument is not only relevant for our calculation but should be relevant for other applications of EDMFT which have focused on discussing the possibility of novel quantum critical points in the presence of two-dimensional magnetic fluctuations.^{38,39} While our reasoning does not apply directly to the quantum critical point, it strongly suggests that no solution exists on the ordered side of the phase diagram below a finite breakdown temperature. While this breakdown temperature will probably vanish at the quantum phase transition, this nevertheless casts some doubt on the applicability of EDMFT at the quantum critical point.

Our formal argument starts from the observation that in two dimensions no phase transition (of first or second order) is possible for $T>0$ within EDMFT, since in a hypothetical ordered phase the local susceptibility would diverge due to the presence of Goldstone modes—in this respect, the EDMFT approach obeys the Mermin-Wagner theorem. Technically, this fact is built into the EDMFT by the self-consistent treatment of the spin fluctuations: A second-order phase transition would require the static spin susceptibility $\chi_{q,\alpha}(0)$, Eq. (3), to diverge at some wave vector \mathbf{q} . In one or two dimensions this would immediately imply a logarithmic or power-law divergence, respectively, of the static local susceptibility, Eq. (9). The latter is forbidden in EDMFT by the self-consistency requirement $\chi_{loc} = \chi_{imp}$, where χ_{imp} —e.g., Eq. (27)—is nondivergent for $T>0$. We mention in passing that even in the case of Ising symmetry a second-order phase transition is not possible, as within EDMFT the longitudinal fluctuations would diverge at the critical point; however, in this case a first-order transition towards an ordered phase for $T>0$ cannot be excluded on general grounds. Indeed, a first-order transition has been found by Sun and Kotliar²¹ and Zhu, Grepel, and Si²⁰ for an Ising-coupled Anderson lattice or Kondo lattice, respectively. Assuming that for $T=0$ the system is magnetically ordered, the local susceptibility $\chi_{loc}(0) \sim \ln \xi$ will grow steadily as T is lowered where ξ is exponentially large, $\xi \sim e^{\beta E^*}$, for $T \ll E^*$ and E^* can crudely be identified with the mean-field transition temperature. However, we have shown that within EDMFT, $\chi''(\omega)$ is bounded from above by the requirements of self-consistency. How can this be reconciled with large $\chi_{loc}(0) = \int [\text{Im} \chi''(\omega)/\omega] d\omega / \pi \sim \ln \xi$? The only possibility consistent with the Kramers-Kronig relation is that $\chi''(\omega)$ is con-

stant down to an *exponentially* small energy scale $E^c(T) \sim 1/\xi^z$, where z is some positive exponent. For sufficiently small T , $E^c(T)$ will be exponentially smaller than T . At this point we have to ask the question whether the solution of the effective impurity model can produce a structure at energies exponentially smaller than T . We think that this is extremely unlikely and conclude therefore that no solution can exist for sufficiently small T , consistent with our results and also with QMC simulations by Burdin *et al.*⁴⁰ of a model equivalent to ours in the limit of zero doping.

Equation (56) also shows how the pseudogap in $M(\omega)$ emerges from the self-consistency of χ and M . The absorptive part of the self-energy M , as seen from Eq. (57), is exponentially small in the regime where

$$8J\chi'(\omega) \gg 1. \quad (59)$$

From the numerical results in Fig. 10 one sees that Eq. (59) is satisfied if $|\omega| < c_M J$, where c_M is a constant of order unity, which depends on the DOS $N_J(\epsilon)$. Thus, the pseudogap is found to develop as a consequence of the increase of $\chi'(0) \propto (1/J) \ln \xi$ with growing ξ , in two dimensions. We stress that a relation similar to Eq. (56) between $M(\omega)$ and $\chi(\omega)$ holds whenever the DOS $N_J(\epsilon)$ is finite at the band edges, which is a signature of two dimensions. In this case the conclusions drawn above remain valid when $1/8J$ is replaced by ΔN_J , the DOS jump, and χ is replaced by $\chi - \chi_{reg}$, where $\chi_{reg}(\omega) = \int d\epsilon \epsilon [N_J(\epsilon) - \Delta N_J] / [J_{\mathbf{q}} + M(\omega)]$.

VI. CONCLUSION

The physics of the doped Mott-Hubbard insulator is governed by the interplay of the motion of holes and the antiferromagnetic fluctuations of the spin background. In this paper we have used a local approximation scheme to describe both the constrained hopping of holes and the quantum spin fluctuations in the paramagnetic phase on an equal footing. The local approximation becomes exact in the limit of infinite coordination number of the underlying lattice and is known as extended dynamical mean-field theory. Rather than studying the model in this limit, we take the point of view that in finite dimensions the approximation of neglecting the momentum dependence of the single-particle self-energy and the J -irreducible spin susceptibility may still be useful. Here we have applied this scheme to the two-dimensional square lattice with nearest-neighbor hopping and exchange interaction. We expect that the approximation should work in a regime of temperatures and doping concentrations where incoherent fluctuations dominate and wash out any of the collective effects sensitive to the system dimension, such as long-range antiferromagnetic order or superconductivity.

In the regime of temperatures above $T \sim 0.1J$ and for doping levels of $0.01 \leq \delta \leq 0.3$, we indeed find a highly incoherent phase, with a broad distribution of spin excitation energies, a high entropy and a large electrical resistance. Most strikingly, the local single-particle spectral function, which is characterized by a narrow peak above the chemical potential for $\delta \geq 0.25$, develops a pseudogap as δ is reduced down to the few percent range. The appearance of the pseudogap is

related to a dramatic shift of the effective chemical potential from its noninteracting (i.e., Fermi liquid) value near the center of the lower Hubbard band to the upper band edge. The shift persists down to the lowest accessible temperatures of $T \approx 0.1J$ and constitutes an unequivocal signal of non-Fermi-liquid behavior in the regime $0.01 \lesssim \delta \lesssim 0.2$. The single-particle pseudogap is accompanied by a gap in the spin excitation spectrum for momenta not too close to the ordering wave vector $Q = (\pi, \pi)$.

The Hall transport is found to be hole like, the Hall constant tending to large positive values $\propto 1/\delta$ as the doping is reduced. At large dopings and low temperatures Fermi-liquid-type behavior is recovered.

These results are encouraging and give rise to the expectation that the present EDMFT scheme is able to capture the main features of the t - J model in the incoherent regime. At lower temperatures and small dopings one should expect the closeness to the antiferromagnetic transition at $T=0$ and $\delta < \delta_c$ to play an important role. We indeed find that the EDMFT equations stop having a physical solution below a limiting temperature of $T \approx 0.1J$. We are able to trace this behavior to an intrinsic lack of structure in the spin structure factor of the effective impurity model, which is ultimately due to the insufficient treatment of critical fluctuations in the EDMFT model. It is likely that similar limitations apply to other applications of the EDMFT in low-dimensional systems.

In conclusion, we emphasize that within the present local approximation scheme neither effects of finite-range, slowly fluctuating antiferromagnetic or superconducting domains nor local singlet formation or similar short-range correlations are included. Nonetheless, the strongly incoherent fluctuations characteristic of our approach (in this case of the spins, but one could imagine similar effects, e.g., in the superconducting sector) suffice to drive pseudogap formation, a violation of Luttinger's theorem, and a hole-type Fermi surface in the proximity of a Mott insulator.

ACKNOWLEDGMENTS

We acknowledge helpful discussions with E. Abrahams, J. Bonča, A. Georges, D.R. Grempel, M. Grilli, P. Howell, G. Kotliar, O. Parcollet, Q. Si, and especially P. Prelovšek. Part of this work was supported by the Ministry of Education, Science and Sport of Slovenia, the FERLIN program of the ESF (K.H.), and the Emmy-Noether program of the Deutsche Forschungsgemeinschaft (A.R.).

APPENDIX A: EDMFT DERIVATION

In this appendix we derive the EDMFT self-consistent equations for the t - J model using the cavity method.

To treat the no-double occupancy constraint of the t - J model, we will add a local Coulomb repulsion term explicitly and take the limit $U \rightarrow \infty$ at the end. In this approach, the electron creation (destruction) operators c_i (c_i^\dagger) obey the usual fermion anticommutation relations. The resulting Hamiltonian is the so-called extended Hubbard model

$$H = - \sum_{ij,\sigma} t_{ij} c_{i\sigma}^\dagger c_{j\sigma} + U \sum_i n_{i\uparrow} n_{i\downarrow} + \frac{1}{2} \sum_{ij} J_{ij} \mathbf{S}_i \cdot \mathbf{S}_j. \quad (\text{A1})$$

It is straightforward to extend the theory to other nonlocal interactions like nonlocal Coulomb repulsion, but since we are mainly interested in the effect of magnetic fluctuations, we will neglect other terms in the Hamiltonian.

For simplicity, let us assume there is no long-range order (i.e., the system is in the paramagnetic state). Let us start the derivation of the EDMFT equations with the action corresponding to the Hamiltonian (A1):

$$S = \int_0^\beta d\tau \left[\sum_{ij,\sigma} c_{i\sigma}^\dagger(\tau) \left(\frac{\partial}{\partial \tau} - \mu \right) \delta_{ij} - t_{ij} \right] c_{j\sigma}(\tau) + \frac{1}{2} \sum_{ij} J_{ij} \mathbf{S}_i(\tau) \cdot \mathbf{S}_j(\tau) + \sum_i U n_{i\uparrow}(\tau) n_{i\downarrow}(\tau) \right]. \quad (\text{A2})$$

The action can be divided into three parts: the on-site part for the chosen site (S_0),

$$S_0 = \int_0^\beta d\tau \left[\sum_\sigma c_{0\sigma}^\dagger(\tau) \left(\frac{\partial}{\partial \tau} - \mu \right) c_{0\sigma}(\tau) + U n_{0\uparrow}(\tau) n_{0\downarrow}(\tau) \right], \quad (\text{A3})$$

the intersite interaction between the chosen site 0 and the rest of the system (ΔS),

$$\Delta S = \int_0^\beta d\tau \left[\sum_{i,\sigma} -t_{i0} c_{i\sigma}^\dagger(\tau) c_{0\sigma}(\tau) - t_{0i} c_{0\sigma}^\dagger(\tau) c_{i\sigma}(\tau) + \frac{1}{2} (J_{i0} + J_{0i}) \mathbf{S}_i(\tau) \cdot \mathbf{S}_0(\tau) \right], \quad (\text{A4})$$

and the lattice action in the presence of the cavity ($S^{(0)}$), which is equal to the original action (A2) with site 0 excluded from all summations.

The series expansion in the coupling between the central site and the rest of the system can be expressed as

$$\begin{aligned} Z &= \int Dc_{0\sigma}^\dagger Dc_{0\sigma} \int \prod_{i \neq 0} Dc_{i\sigma}^\dagger Dc_{i\sigma} \\ &\times \exp \left(-S_0 - S^{(0)} - \int_0^\beta \Delta \mathcal{L}(\tau) d\tau \right) \\ &= \int Dc_{0\sigma}^\dagger Dc_{0\sigma} \exp(-S_0) Z^{(0)} \left(1 - \int_0^\beta \langle \Delta \mathcal{L}(\tau) \rangle^{(0)} d\tau \right. \\ &\quad \left. + \frac{1}{2!} \int_0^\beta d\tau_1 \int_0^\beta d\tau_2 \langle T_\tau \Delta \mathcal{L}(\tau_1) \Delta \mathcal{L}(\tau_2) \rangle^{(0)} + \dots \right), \end{aligned} \quad (\text{A5})$$

where $\Delta S = \int_0^\beta \Delta \mathcal{L}(\tau) d\tau$ and $\langle \rangle^{(0)}$ means the average with respect to the cavity action $S^{(0)}$. In the second line we have integrated out all fermions except for site 0.

The first term linear in $\Delta \mathcal{L}$ vanishes, since the average of each spin $\langle \mathbf{S}_i(\tau) \rangle = 0$ is zero by the assumption of no long-range order in the system. For the broken-symmetry phase,

the spin operator has to be replaced with its deviation from the average value $\mathbf{S}_i \rightarrow \mathbf{S}_i - \langle \mathbf{S}_i \rangle$ and the derivation can proceed along the same lines. The second term in the series expansion reads

$$\begin{aligned} & \frac{1}{2!} \int_0^\beta d\tau_1 \int_0^\beta d\tau_2 \langle T_\tau \Delta \mathcal{L}(\tau_1) \Delta \mathcal{L}(\tau_2) \rangle^{(0)} \\ &= \frac{1}{2!} \int_0^\beta d\tau_1 \int_0^\beta d\tau_2 \left\langle T_\tau \left[\sum_{i,\sigma} t_{i0} c_{i\sigma}^\dagger(\tau_1) c_{0\sigma}(\tau_1) \right. \right. \\ & \quad \left. \left. + t_{0i} c_{0\sigma}^\dagger(\tau_1) c_{i\sigma}(\tau_1) - \sum_i J_{0i} \mathbf{S}_0(\tau_1) \cdot \mathbf{S}_i(\tau_1) \right] \right. \\ & \quad \left. \times \left[\sum_{i,\sigma} t_{i0} c_{i\sigma}^\dagger(\tau_2) c_{0\sigma}(\tau_2) + t_{0i} c_{0\sigma}^\dagger(\tau_2) c_{i\sigma}(\tau_2) \right. \right. \\ & \quad \left. \left. - \sum_i J_{i0} \mathbf{S}_i(\tau_2) \cdot \mathbf{S}_0(\tau_2) \right] \right\rangle^{(0)}. \end{aligned} \quad (\text{A7})$$

It is crucial to observe that there is no interference between the kinetic and the spin term since the average of the correlation function $\langle c_{i\sigma}(\tau_1) \mathbf{S}_j(\tau_2) \rangle^{(0)}$ vanishes. The leading-order term in the effective action thus reads

$$\begin{aligned} S_{\text{eff}} &= S_0 - \int \int_0^\beta d\tau_1 d\tau_2 \\ & \times \left[c_{0\sigma}^\dagger(\tau_1) \sum_{ij} t_{i0} t_{0j} \langle T_\tau c_{i\sigma}(\tau_1) c_{j\sigma}^\dagger(\tau_2) \rangle^{(0)} c_{0\sigma}(\tau_2) \right. \\ & \quad \left. + \mathbf{S}_0(\tau_1) \frac{1}{2} \sum_{ij} J_{i0} J_{0j} \langle T_\tau \mathbf{S}_i(\tau_1) \mathbf{S}_j(\tau_2) \rangle^{(0)} \mathbf{S}_0(\tau_2) \right]. \end{aligned} \quad (\text{A8})$$

Within EDMFT both terms are equally important and are of order 1 in the $1/d$ expansion. The two-point Green's function and the susceptibility scale as $1/d^{|i-j|/2}$ since t and J fall off as $1/\sqrt{d}$. Furthermore i and j are neighbors of site 0 and are thus at least 2 lattice sites apart (in Manhattan distance) giving a contribution of order $1/d$. The prefactor t^2 or J^2 is proportional to $1/d$, while the double sum gives d^2 and the net result is therefore of order 1.

Further it follows from the linked cluster theorem that only *connected* n -point correlation functions appear in higher-order terms of the effective action. Since they have the usual dependence on $1/d$, all but the first term vanish in the limit $d \rightarrow \infty$. For instance, the next-order term would involve three-point connected correlation functions $\chi_{ijk} \sim \langle S_i^z S_j^z S_k^z \rangle$ or $C_{ijk} \sim \langle S_i^z c_j^\dagger c_k \rangle$ that scale like $1/d^{|i-j|/2} d^{|i-k|/2}$. When all three variables i, j , and k are different, the correlation functions is of order $1/d^2$ since all three sites are neighbors of 0. The prefactor J^3 or Jt^2 is proportional to $1/d^{3/2}$ while the sums give d^3 . The term is thus of order $1/\sqrt{d}$. If $i=j$, but distinct from k , the correlation function is of order $1/d$ while sums give d^2 and the net result is again of order $1/\sqrt{d}$. Higher-order terms fall off

faster than $1/\sqrt{d}$. Thus, in the limit of large d all but the first term (A8) can be neglected and the effective action becomes

$$\begin{aligned} S_{\text{eff}} &= \int_0^\beta U n_{0\uparrow}(\tau) n_{0\downarrow}(\tau) \\ & - \int_0^\beta d\tau_1 \int_0^\beta d\tau_2 c_{0\sigma}^\dagger(\tau_1) \mathcal{G}_0^{-1}(\tau_1 - \tau_2) c_{0\sigma}(\tau_2) \\ & - \frac{1}{2} \int_0^\beta d\tau_1 \int_0^\beta d\tau_2 \mathbf{S}_0(\tau_1) \underline{\chi}_0^{-1}(\tau_1 - \tau_2) \mathbf{S}_0(\tau_2), \end{aligned} \quad (\text{A9})$$

where

$$\mathcal{G}_0^{-1}(i\omega) = i\omega + \mu - \sum_{ij} t_{i0} t_{0j} G_{ij}^{(0)}(i\omega),$$

$$\chi_0^{-1}(i\omega) = \sum_{ij} J_{i0} J_{0j} \chi_{ij}^{(0)}(i\omega). \quad (\text{A10})$$

The Weiss fields are thus determined by the cavity Green's function $G_{ij}^{(0)}$ and the cavity susceptibility $\chi_{ij}^{(0)}$. The absence of interference between the kinetic and spin terms in Eq. (A8) also leads to separate equations for both cavity quantities:

$$\begin{aligned} G_{ij}^{(0)} &= G_{ij} - G_{i0} G_{00}^{-1} G_{0j}, \\ \chi_{ij}^{(0)} &= \chi_{ij} - \chi_{i0} \chi_{00}^{-1} \chi_{0j}. \end{aligned} \quad (\text{A11})$$

Using power-counting arguments one can show^{5,6} that in the limit $d \rightarrow \infty$ and EDMFT scaling the single-particle self-energy $\Sigma(i\omega)$ as well as the double particle self-energy $M(i\omega)$ become local quantities, i.e.,

$$\begin{aligned} G_{\mathbf{k}}(i\omega) &= \frac{1}{i\omega + \mu - \epsilon_{\mathbf{k}} - \Sigma(i\omega)}, \\ \chi_{\mathbf{q}}(i\omega) &= \frac{1}{J_{\mathbf{q}} + M(i\omega)}. \end{aligned} \quad (\text{A12})$$

Inserting the definitions (A12) into (A11) and combining with Eqs. (A10) we finally obtain the self-consistent conditions

$$\begin{aligned} \mathcal{G}_0^{-1} &= \Sigma + G_{loc}^{-1}, \\ \chi_0^{-1} &= M - \chi_{loc}^{-1}. \end{aligned} \quad (\text{A13})$$

These relate the Weiss fields to the local quantities computable from the local action (A9). The system of equations is thus closed.

For practical computation, however, it is convenient to have a Hamiltonian representation of the local effective action (A9). Since it includes retardation effects through frequency dependent Weiss fields, it is necessary to introduce auxiliary degrees of freedom describing the baths. The one-particle character of the Weiss field \mathcal{G}_0^{-1} can be represented

with the fermionic bath while the two particle field χ_0^{-1} has a bosonic nature and dictates a bosonic bath. One of the possible choices is

$$H = \sum_{k\sigma} E_k c_{k\sigma}^\dagger c_{k\sigma} + V \sum_{k\sigma} (c_{k\sigma}^\dagger c_{0\sigma} + c_{0\sigma}^\dagger c_{k\sigma}) - \sum_{\sigma} \mu c_{0\sigma}^\dagger c_{0\sigma} + U n_{0\uparrow} n_{0\downarrow} + \sum_q \omega_q \mathbf{h}_q^\dagger \cdot \mathbf{h}_q + I \sum_q \mathbf{S}_0 \cdot (\mathbf{h}_q + \mathbf{h}_{-q}^\dagger), \quad (\text{A14})$$

where \mathbf{h}_q corresponds to a vector-bosonic bath with the commutation relations $[h_q^\alpha, h_{q'}^{\beta\dagger}] = \delta_{qq'} \delta_{\alpha\beta}$. The corresponding action

$$S = S_0 + \int_0^\beta d\tau \sum_{k\sigma} \left[c_{k\sigma}^\dagger(\tau) \left(\frac{\partial}{\partial \tau} + E_k \right) c_{k\sigma}(\tau) + V c_{k\sigma}^\dagger(\tau) c_{0\sigma}(\tau) + V c_{0\sigma}^\dagger(\tau) c_{k\sigma}(\tau) \right] + \int_0^\beta d\tau \sum_q \left[\mathbf{h}_q^\dagger(\tau) \left(\frac{\partial}{\partial \tau} + \omega_q \right) \mathbf{h}_q(\tau) + I \mathbf{h}_q(\tau) \cdot \mathbf{S}_0(\tau) + I \mathbf{S}_0(\tau) \cdot \mathbf{h}_{-q}^\dagger(\tau) \right] \quad (\text{A15})$$

is quadratic in $c_{k\sigma}$ and \mathbf{h}_q , and therefore both baths can be eliminated, leading to

$$S = S_0 - \int_0^\beta d\tau_1 \int_0^\beta d\tau_2 \sum_{\sigma} c_{0\sigma}^\dagger(\tau_1) \left(\sum_k V^2 \frac{\delta_{\tau_1 \tau_2}}{\frac{\partial}{\partial \tau} + E_k} \right) c_{0\sigma}(\tau_2) - \int_0^\beta d\tau_1 \int_0^\beta d\tau_2 \mathbf{S}_0(\tau_1) \left(\sum_q I^2 \frac{\delta_{\tau_1 \tau_2}}{\frac{\partial}{\partial \tau} + \omega_q} \right) \mathbf{S}_0(\tau_2). \quad (\text{A16})$$

This action is identical to the effective action (A9) provided that the following relations hold:

$$\mathcal{G}_0^{-1}(\tau_1 - \tau_2) = - \left(\frac{\partial}{\partial \tau_1} - \mu \right) \delta_{\tau_1 \tau_2} + \sum_k V^2 \frac{\delta_{\tau_1 \tau_2}}{\frac{\partial}{\partial \tau} + E_k},$$

$$\chi_0^{-1}(\tau_1 - \tau_2) = \sum_q I^2 \left(\frac{\delta_{\tau_1 \tau_2}}{\frac{\partial}{\partial \tau} + \omega_q} + \frac{\delta_{\tau_1 \tau_2}}{-\frac{\partial}{\partial \tau} + \omega_q} \right), \quad (\text{A17})$$

or, equivalently,

$$\mathcal{G}_0^{-1}(i\omega) = i\omega + \mu - V^2 G_c(i\omega),$$

$$\chi_0^{-1}(i\omega) = -I^2 G_h(i\omega). \quad (\text{A18})$$

Finally, combining Eqs. (A13) and (A18) yields

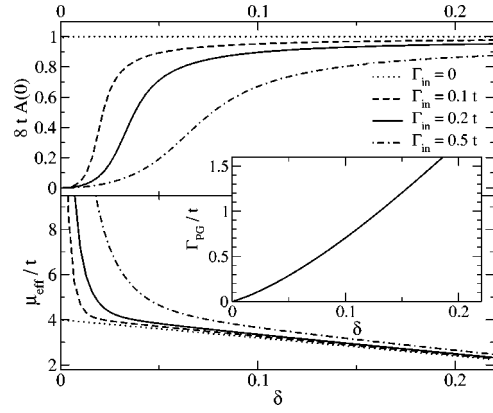


FIG. 21. Upper panel: normalized spectral density at $\omega=0$ as a function of hole doping δ for a toy model of a doped band insulator (see text) and various values of Γ_{in} . For large Γ_{in} and small doping the density of states is reduced. The origin of this effect is that the effective chemical potential, shown in the lower panel, moves outside of the band edge $4t$. Inset: Γ_{PG} as a function of doping. For $\Gamma_{\text{in}} > \Gamma_{\text{PG}}$ the density of states at $\omega=0$ is reduced by more than a factor of 1/2.

$$G_{\text{loc}}^{-1} = i\omega + \mu - \Sigma - V^2 G_c,$$

$$\chi_{\text{loc}}^{-1} = M + I^2 G_h, \quad (\text{A19})$$

which coincide with Eqs. (10) and (11).

APPENDIX B: PSEUDOGAPS IN A DOPED BAND AND MOTT INSULATOR

In this appendix we investigate in the framework of simplified models, first, how a pseudogap is generated in a doped Mott (or band) insulator when the chemical potential μ_{eff} moves up to and beyond the bare band edge and, second, how strong incoherence drives the chemical potential far out of the bare band for a doped *band* insulator.

Using a flat bare density of states with $N(\epsilon_{\mathbf{k}}) = (1/8t)\Theta(4t - |\epsilon_{\mathbf{k}}|)$, the local Green's function (8) is given by

$$G_{\text{loc}}(\omega) = \frac{1}{8t} \ln \left(\frac{\omega + \mu - \Sigma(\omega) + 4t}{\omega + \mu - \Sigma(\omega) - 4t} \right). \quad (\text{B1})$$

At $\omega=0$, defining $\mu_{\text{eff}} = \mu - \text{Re} \Sigma(0)$ and $\text{Im} \Sigma(0) = -\Gamma_{\text{in}}$, the local density of states is obtained from Eq. (B1) as

$$A_{\text{loc}}(0) = \frac{1}{8t} \left[\frac{1}{2} - \frac{1}{\pi} \arctan \left(\frac{\mu_{\text{eff}}^2 + \Gamma_{\text{in}}^2 - 16t^2}{8t\Gamma_{\text{in}}} \right) \right]. \quad (\text{B2})$$

In the Fermi liquid regime, when $\mu_{\text{eff}}^2 + \Gamma_{\text{in}}^2 \ll 16t^2$ and $\Gamma_{\text{in}} \ll 4t$, $A_{\text{loc}}(0) \approx 1/8t$. As μ_{eff} moves towards the band edge, $A_{\text{loc}}(0)$ is strongly reduced, at $\mu_{\text{eff}} = \sqrt{16t^2 - \Gamma_{\text{in}}^2}$ by a factor of 1/2, and $A_{\text{loc}}(0)$ drops to zero for μ_{eff} far above the band (see Fig. 21 and discussion below). This simple observation is the main reason why we obtain a reduced density of states in the incoherent regime at small dopings. In order to understand the origin of the rather sharp threshold behavior in $A_{\text{loc}}(\omega)$ at $\omega = -J$ in Figs. 2 and 3 better, it is useful to

analyze the model given above, now allowing for ω -dependent Σ . For small ω we may still neglect the ω dependence of $\text{Im } \Sigma(\omega)$, but keep it for $\text{Re } \Sigma$ in the approximate form $\omega + \mu - \text{Re } \Sigma(\omega) \approx \omega/Z + \mu_{\text{eff}}$, where the Z factor has been defined in Eq. (33). From Fig. 6, we see that $1/Z \approx 3-5$, leading to a rapid reduction of $\omega + \mu - \text{Re } \Sigma(\omega)$ for negative ω from μ_{eff} to values below $\sqrt{16t^2 - \Gamma_{\text{in}}^2}$. This leads to a rapid increase of $A_{\text{loc}}(\omega)$ for negative ω as found in Figs. 2 and 3.

We now address the question of why μ_{eff} moves up to and even outside the bare band for small doping and increasing scattering. We study this question in the case of a doped band insulator with (unspecified) inelastic scattering, assuming a model form for the self energy, $\Sigma(\omega) = -i\Gamma_{\text{in}}$. In a Mott insulator the ω dependence of $\Sigma(\omega)$ is much more complicated and a simple ‘‘toy-model’’ form is not known to us. The effective chemical potential is determined from the particle number condition (at low temperatures, $T \ll \Gamma_{\text{in}}$)

$$1 - \delta = - \int_{-\infty}^0 \text{Im}[G_{\text{loc}}(\omega)] \frac{d\omega}{\pi}. \quad (\text{B3})$$

The result of solving Eq. (B3) for μ_{eff} (equal to μ in this case) for fixed Γ_{in} as a function of hole doping δ is shown in the lower part of Fig. 21: Due to the tails in the local density of states induced by Γ_{in} , the effective chemical potential μ_{eff} has to move far above the band for decreasing δ to be consistent with Eq. (B3); for $\delta \rightarrow 0$ we obtain $\mu \approx 4t \coth[4t\pi\delta\Gamma_{\text{in}}] \approx \Gamma_{\text{in}}/\pi\delta$. As a consequence, the local spectral function at the Fermi level gets very small for decreasing δ (upper panel of Fig. 21) with

$$A(0) \approx \frac{\Gamma_{\text{in}}}{16\pi t^2} \sinh^2 \left[\frac{4t\pi\delta}{\Gamma_{\text{in}}} \right] \approx \pi \frac{\delta^2}{\Gamma_{\text{in}}} \quad \text{for } \delta \rightarrow 0.$$

It is useful to determine the value of Γ_{in} at which the pseudogap starts to form for a given δ , named Γ_{PG} in the inset of Fig. 21. Γ_{PG} increases monotonically from zero with increasing δ with

$$\delta \approx \frac{\Gamma_{\text{PG}}}{8t\pi} \ln \left[\frac{8te}{\Gamma_{\text{PG}}} \right] \quad (\text{B4})$$

for small δ . For small dopings rather weak inelastic scattering is sufficient to reduce strongly the density of states at the Fermi energy.

APPENDIX C: SUM RULE CONSTRAINTS ON V^2 AND I^2

Within EDMFT, the coupling parameters V and I defined by Eq. (6), describing the hopping onto and the exchange interaction with the impurity, are determined self-consistently. Interestingly, sum rules completely determine the values of V and partially constrain the values of I . We start with the single-particle hopping V . Defining a complex variable $z = \omega + \mu + \Sigma(\omega - i0)$ one may write the EDMFT self-consistency condition (7), using Eqs. (2), (8), and (10), as

$$H(z) \equiv \int \frac{D(\epsilon) d\epsilon}{z - \epsilon} = \frac{1}{z - V^2 G_c(\omega - i0)}, \quad (\text{C1})$$

with $D(\epsilon)$ the DOS of the tight-binding band $\epsilon_{\mathbf{k}}$ and $G_c(\omega)$ the fermionic bath Green’s function defined in Eq. (12). Solving Eq. (C1) for $V^2 G_c$ and taking the limit $\omega \rightarrow \infty$ one finds

$$\begin{aligned} \lim_{\omega \rightarrow \infty} [\omega V^2 G_c(\omega - i0)] &= V^2 = \lim_{\omega \rightarrow \infty} \left(z - \frac{1}{H(z)} \right) \\ &= \lim_{\omega \rightarrow \infty} \frac{\omega}{z} \langle \epsilon^2 \rangle. \end{aligned} \quad (\text{C2})$$

Here the zero of energy has been chosen such that $\langle \epsilon \rangle = 0$, with $\langle \epsilon^n \rangle = \int d\epsilon D(\epsilon) \epsilon^n$, and $\langle \epsilon^2 \rangle$ is a measure of the squared width of the band. For the tight-binding band $\epsilon_{\mathbf{k}} = 2t(\cos k_x + \cos k_y)$ one finds $\langle \epsilon^2 \rangle = 4t^2$.

We now use the sum rule on the spectral weight in the lower Hubbard band,

$$n_L = \int_{-\infty}^{\infty} \frac{d\omega}{\pi} \text{Im } G_{\text{loc}}(\omega - i0) = \frac{1}{2}(1 + \delta), \quad (\text{C3})$$

which, using the analyticity of $G_c(\omega - i0)$ in the lower half-plane, is equivalent to the statement

$$n_L = \lim_{\omega \rightarrow \infty} \omega G_{\text{loc}}(\omega - i0) = \lim_{\omega \rightarrow \infty} \frac{1}{N_L} \sum_{\mathbf{k}} \frac{\omega}{z - \epsilon_{\mathbf{k}}} = \lim_{\omega \rightarrow \infty} \frac{\omega}{z}, \quad (\text{C4})$$

where N_L is the number of \mathbf{k} points in the first Brillouin zone, which are summed over. Combining Eqs. (C2)–(C4) one gets

$$V^2 = \frac{1}{2}(1 + \delta) \langle \epsilon^2 \rangle. \quad (\text{C5})$$

The coupling constant I may be related to $\chi_{\text{loc}}(\omega)$ and $M(\omega)$. Using Eq. (11), one may express G_h as

$$I^2 G_h(\omega) = M(\omega) - \chi_{\text{loc}}^{-1}(\omega). \quad (\text{C6})$$

Since G_h is a boson Green’s function [see Eq. (13)] with positive energy spectrum, $\omega_q \geq 0$, the following relation holds:

$$\int_0^{\infty} \frac{d\omega}{\pi} \text{Im } G_h(\omega - i0) = 1. \quad (\text{C7})$$

From Eq. (C7) one then finds

$$I^2 = \int_0^{\infty} \frac{d\omega}{\pi} \text{Im}[M(\omega - i0) - \chi_{\text{loc}}^{-1}(\omega - i0)]. \quad (\text{C8})$$

A further relation is obtained by using the f -sum rules:

$$\int \frac{d\omega}{\pi} \omega \text{Im } G_h(\omega - i0) = \lim_{\omega \rightarrow \infty} \omega^2 G_h(\omega) = \frac{1}{N_L} \sum_{\mathbf{q}} 2\omega_{\mathbf{q}} \equiv \bar{\omega}_{\mathbf{q}} \quad (\text{C9})$$

and

$$\int \frac{d\omega}{\pi} \chi''_{loc}(\omega) = \lim_{\omega \rightarrow \infty} \omega^2 \chi_{loc}(\omega). \quad (\text{C10})$$

Taking the limit $\lim_{\omega \rightarrow \infty} \omega^2[\dots]$ of Eq. (C6) one finds

$$\bar{\omega}_{\mathbf{q}} = \frac{\langle \epsilon^2 \rangle}{2I^2} \int \frac{d\omega}{\pi} \omega \chi''_{loc}(\omega), \quad (\text{C11})$$

with $\langle \epsilon^2 \rangle$ as defined after Eq. (C2).

-
- ¹P.W. Anderson, *The Theory of Superconductivity in the High T_c Cuprates* (Princeton University Press, Princeton, 1997).
- ²S. Chakravarty, B.I. Halperin, and D.R. Nelson, *Phys. Rev. B* **39**, 2344 (1989).
- ³B.B. Beard, R.J. Birgeneau, M. Greven, and U.-J. Wiese, *Phys. Rev. Lett.* **80**, 1742 (1998).
- ⁴W. Metzner and D. Vollhardt, *Phys. Rev. Lett.* **62**, 324 (1989).
- ⁵A. Georges, G. Kotliar, W. Krauth, and M.J. Rozenberg, *Rev. Mod. Phys.* **68**, 13 (1996).
- ⁶Q. Si and J.L. Smith, *Phys. Rev. Lett.* **77**, 3391 (1996); J.L. Smith and Q. Si, *Phys. Rev. B* **61**, 5184 (2000).
- ⁷H. Kajüter, Ph.D. thesis, Rutgers University, 1996.
- ⁸T.A. Costi, J. Kroha, and P. Wölfle, *Phys. Rev. B* **53**, 1850 (1996).
- ⁹J. Kroha, and P. Wölfle, in *Theoretical Methods for Strongly Correlated Electrons*, edited by D. Sénéchal, A.-M. Tremblay, and C. Bourbonnais, CRM Series in Mathematical Physics (Springer, New York, 2003); cond-mat/0105491 (unpublished).
- ¹⁰N.E. Bickers, *Rev. Mod. Phys.* **59**, 845 (1987).
- ¹¹A. Ino, C. Kim, M. Nakamura, T. Yoshida, T. Mizokawa, A. Fujimori, Z.-X. Shen, T. Kakeshita, H. Eisaki, and S. Uchida, *Phys. Rev. B* **65**, 094504 (2002); J.C. Campuzano, H. Ding, M.R. Norman, and M. Randeria, *Physica B* **259–261**, 517 (1999).
- ¹²T. Timusk and B. Statt, *Phys. Rep.* **62**, 61 (1999).
- ¹³J.L. Tallon and J.W. Loram, *Physica C* **349**, 53 (2001).
- ¹⁴J.R. Cooper and J.W. Loram, *J. Phys. I* **6**, 2237 (1996); Y. Ando, K. Segawa, A.N. Lavrov, and S. Komiya, *J. Low Temp. Phys.* **131**, 793 (2003).
- ¹⁵K. Haule, A. Rosch, J. Kroha, and P. Wölfle, *Phys. Rev. Lett.* **89**, 236402 (2002).
- ¹⁶Th.A. Maier, Th. Pruschke, and M. Jarrell, *Phys. Rev. B* **66**, 075102 (2002); Th.A. Maier, M. Jarrell, A. Macridin, and F.-C. Zhang, cond-mat/0208419 (unpublished); C. Huscroft, M. Jarrell, Th. Maier, S. Moukouri, and A.N. Tahvildarzadeh, *Phys. Rev. Lett.* **86**, 139 (2001).
- ¹⁷T.D. Stanescu and P. Phillips, cond-mat/0301254 (unpublished); cond-mat/0209118 (unpublished).
- ¹⁸A. Rosch, *Phys. Rev. B* **64**, 174407 (2001) and references therein.
- ¹⁹R. Bulla, A.C. Hewson, and Th. Pruschke, *J. Phys.: Condens. Matter* **10**, 8365 (1998); R. Bulla, *Adv. Solid State Phys.* **40**, 169 (2000).
- ²⁰D.R. Grempel and Qimiao Si, *Phys. Rev. Lett.* **91**, 026401 (2003); J.-X. Zhu, D.R. Grempel, and Qimiao Si, cond-mat/0304033, *Phys. Rev. B* (to be published).
- ²¹P. Sun and G. Kotliar, *Phys. Rev. B* **66**, 085120 (2002); *Phys. Rev. Lett.* **91**, 037209 (2003).
- ²²S.E. Barnes, *J. Phys. F: Met. Phys.* **6**, 1375 (1976); *ibid.* **7**, 2637 (1977).
- ²³A.A. Abrikosov, *Physics* (Long Island City, N.Y.) **2**, 21 (1965).
- ²⁴O. Parcollet and A. Georges, *Phys. Rev. B* **59**, 5341 (1999).
- ²⁵S. Sachdev and J. Ye, *Phys. Rev. Lett.* **70**, 3339 (1993).
- ²⁶T.A. Costi, P. Schmitteckert, J. Kroha, and P. Wölfle, *Phys. Rev. Lett.* **73**, 1275 (1994).
- ²⁷E. Manousakis, *Rev. Mod. Phys.* **63**, 1 (1991).
- ²⁸J. Jaklič and P. Prelovšek, *Adv. Phys.* **49**, 1 (2000).
- ²⁹J.W. Loram, K.A. Mirza, J.R. Cooper, N.A. Athanassopoulou, and W.Y. Lian, in *Proceedings of the 10th Anniversary HTS Workshop, Houston, 1996*, edited by B. Batlogg, C.W. Chu, W.K. Chu, D.U. Gubser, and K.A. Muller (World Scientific, Singapore, 1996), p. 341.
- ³⁰M. Imada, A. Fujimori, and Y. Tokura, *Rev. Mod. Phys.* **70**, 1039 (1998).
- ³¹E. Müller-Hartmann, *Z. Phys. B: Condens. Matter* **74**, 507 (1989).
- ³²A. Khurana, *Phys. Rev. Lett.* **64**, 1990 (1990).
- ³³H. Kohno and K. Yamada, *Prog. Theor. Phys.* **80**, 623 (1988).
- ³⁴P. Voruganti, A. Golubentsev, and S. John, *Phys. Rev. B* **45**, 13 945 (1992).
- ³⁵E. Lange and G. Kotliar, *Phys. Rev. Lett.* **82**, 1317 (1991).
- ³⁶P. Prelovšek, *Phys. Rev. B* **55**, 9219 (1997).
- ³⁷T. Pruschke, D.L. Cox, and M. Jarrell, *Phys. Rev. B* **47**, 3553 (1993).
- ³⁸Q. Si, S. Rabello, K. Ingersent, and J.L. Smith, *Nature* (London) **413**, 804 (2001).
- ³⁹D.R. Grempel and Qimiao Si, cond-mat/0207493 (unpublished).
- ⁴⁰S. Burdin, M. Grilli, and D.R. Grempel, *Phys. Rev. B* **67**, 121104 (2003).
- ⁴¹T. Nishikana, J. Takeda, and M. Sata, *J. Phys. Soc. Jpn.* **63**, 1441 (1994).